The Astrophysical Journal, 604:741–757, 2004 April 1
© 2004. The American Astronomical Society. All rights reserved. Printed in U.S.A.

AN ASSESSMENT OF DYNAMICAL MASS CONSTRAINTS ON PRE–MAIN-SEQUENCE EVOLUTIONARY TRACKS

Lynne A. Hillenbrand and Russel J. White
Department of Astronomy, California Institute of Technology, Mail Code 105-24, Pasadena, CA 91125
Received 2003 September 8; accepted 2003 December 12

ABSTRACT

We have assembled a database of stars having both masses determined from measured orbital dynamics and sufficient spectral and photometric information for their placement on a theoretical H-R diagram. Our sample consists of 115 low-mass ($M < 2.0\ M_{\odot}$) stars, 27 pre–main-sequence and 88 main-sequence. We use a variety of available pre–main-sequence evolutionary calculations to test the consistency of predicted stellar masses with dynamically determined masses. Despite substantial improvements in model physics over the past decade, large systematic discrepancies still exist between empirical and theoretically derived masses. For main-sequence stars, all models considered predict masses consistent with dynamical values above 1.2 $M_{\odot}$ and some models predict consistent masses at solar or slightly lower masses, but no models predict consistent masses below 0.5 $M_{\odot}$, with all models systematically underpredicting such low masses by 5%–20%. The failure at low masses stems from the poor match of most models to the empirical main sequence below temperatures of 3800 K, at which molecules become the dominant source of opacity and convection is the dominant mode of energy transport. For the pre–main-sequence sample we find similar trends. There is generally good agreement between predicted and dynamical masses above 1.2 $M_{\odot}$ for all models. Below 1.2 $M_{\odot}$ and down to 0.3 $M_{\odot}$ (the lowest mass testable), most evolutionary models systematically underpredict the dynamically determined masses by 10%–30%, on average, with the Lyon group models predicting marginally consistent masses *in the mean*, although with large scatter. Over all mass ranges, the usefulness of dynamical mass constraints for pre–main-sequence stars is in many cases limited by the *random* errors caused by poorly determined luminosities and especially temperatures of young stars. Adopting a warmer-than-dwarf temperature scale would help reconcile the *systematic* pre–main-sequence offset at the lowest masses, but the case for this is not compelling, given the similar warm offset at older ages between most sets of tracks and the empirical main sequence. Over all age ranges, the systematic discrepancies between track-predicted and dynamically determined masses appear to be dominated by inaccuracies in the treatment of convection and in the adopted opacities.

Subject headings: binaries: general — Hertzsprung-Russell diagram — stars: pre–main-sequence

On-line material: machine-readable table, color figures

1. INTRODUCTION

Three of the most fundamental stellar parameters are mass, angular momentum, and composition, which together determine almost exclusively the entire evolutionary history of any given (single) star. Although stars spend the vast majority of their lives on the main sequence of hydrogen burning, particularly interesting stellar objects are often those in the shorter-lived pre– or post–main-sequence evolutionary phases. Our focus here is on the inference of stellar masses for pre–main-sequence and young main-sequence objects, for which observational data relevant to their location in the Hertzsprung-Russell (H-R) diagram have become abundant in recent years. Masses and ages are often inferred from such H-R diagrams via comparisons to an increasingly large suite of pre–main-sequence evolutionary calculations. Instead of adopting a main-sequence mass-luminosity relationship, one explicitly accounts for the evolution of the mass-luminosity relationship with age. The inferred stellar masses and ages are then used to construct initial mass functions and to surmise star formation histories in stellar associations.

The pre–main-sequence luminosity and effective temperature evolution of just-born stars was first calculated over a range of masses by Iben (1965) and by Ezer & Cameron (1967a, 1967b), who assumed homologous contraction and solved the equations of stellar structure following the formalism of pioneers Henyey and Hayashi. Substantial improvements in the input physics and opacities were achieved during the following decades by several others, notably VandenBerg (1983) and D'Antona & Mazzitelli (1985). In the 1990s several series of papers by different groups incorporated yet more complex and varied assumptions regarding the equation of state, opacities, convection physics, outer boundary condition of the stellar interior, and treatment of atmospheres. Electronically available data from these calculations, including those from Swenson et al. (1994; S93 models); D'Antona & Mazzitelli (1994, 1997; DM94 and DM97 models, respectively); Forestini (1994), Siess, Forestini, & Bertout (1997), and Siess, Dufour, & Forestini (2000; S00 models); Baraffe et al. (1998; B98 models) and Chabrier et al. (2000); Palla & Stahler (1993, 1999; PS99 models); and finally Yi, Kim, & Demarque (2003; Y^2 models), were widely circulated. Other authors, such as Burrows et al. (1997) and Baraffe et al. (2002), have focused on sub–stellar mass objects.

Complications to simple luminosity and effective temperature evolution via radial contraction are the effects of rotation, composition, accretion, magnetic fields, and the presence of dust in the atmospheres of the lowest mass stars and brown dwarfs. These have been explored in a limited capacity as well, as discussed by Mendes, D'Antona, & Mazzitelli (1999),

D'Antona, Ventura, & Mazzitelli (2000), Baraffe et al. (2002), Siess & Livio (1997), and Siess et al. (1997). In addition, the "zero point," or initial mass-radius relationship, from which pre–main-sequence evolution begins is poorly constrained (see Larson 1972; Stahler 1983; Mercer-Smith, Cameron, & Epstein 1984; Palla & Stahler 1993; Bernasconi 1996; Hartmann, Cassen, & Kenyon 1997; Baraffe et al. 2002). Comparison between young cluster data and isochrones, including lithium-burning predictions, show inconsistencies that lead us to infer that ages younger than $\sim$10 Myr are particularly uncertain and that masses are also likely biased. Despite the large uncertainties and, indeed, the cautions offered by many of the above authors themselves regarding the utility of their models in explaining observations, the existing array of models has been used heavily over the past decade for comparison to the H-R diagrams assembled for pre–main-sequence stars in nearby star-forming regions. These tracks are the primary tool used to determine the ages and masses of young stars and thus a cornerstone on which the conclusions of many star formation studies rest. Examples include the interpretation of observational data in a metacontext, such as the initial mass function, the star formation history of a particular region, or the evolution of circumstellar disks or stellar angular momentum through the pre–main sequence. Such conclusions rely entirely on the evolutionary models, and systematically different results can arise from the use of different models.

Fundamental calibration of pre–main-sequence evolutionary tracks is, however, not yet established. Several tests have been proposed. The predicted masses can be compared with those inferred from either binary orbits (e.g., Casey et al. 1998; Covino et al. 2000; Steffen et al. 2001) or velocity profiles of rotating circumstellar disks (e.g., Simon, Dutrey, & Guilloteau 2000; Dutrey, Guilloteau, & Simon 2003). The predicted ages can be compared, under the assumption of coeval formation, with loci of pre–main-sequence binaries (e.g., Hartigan, Strom, & Strom 1994; Prato, Greene, & Simon 2003), higher order multiples (White et al. 1999), and young "star-forming" clusters (e.g., Luhman et al. 2003; L. A. Hillenbrand, M. R. Meyer, & J. M. Carpenter 2004, in preparation). Older open clusters offer even narrower sequences for comparison with model isochrones (e.g., Stauffer, Hartmann, & Barrado y Navascués 1995). All of these tests, however, are limited by the accuracy with which individual stars can be placed on a theoretical H-R diagram. In addition to the poorly understood observational errors, uncertainties in the temperature and bolometric correction scales themselves remain significant, especially at subsolar masses and young ages.

In this paper we explore the consistency of the masses predicted by various sets of pre–main-sequence evolutionary tracks with those masses fundamentally determined from orbital dynamics. Our sample is larger than those considered in previous experiments (referenced above); in particular, we include both pre–main-sequence and main-sequence stars. The lower mass limit in our sample is imposed by the available fundamental mass data (0.1 $M_{\odot}$ for main-sequence stars but only 0.3 $M_{\odot}$ for pre–main-sequence stars), and the upper limit (2.0 $M_{\odot}$) is adopted to include only unevolved main-sequence objects.

In § 2 we discuss the models we test and the systematic differences between them. Section 3 presents the database of double-lined binaries or single/multiple stars harboring rotating gaseous disks with determined stellar masses and our methodology for inferring masses from pre–main-sequence evolutionary calculations. In § 4 we perform the detailed comparison of the model masses and the dynamically determined fundamental masses. Section 5 contains our conclusions and recommendations.

2. PRE–MAIN-SEQUENCE EVOLUTIONARY MODELS

The various sets of tracks available and their most basic input assumptions regarding stellar interior structure and physics are reviewed in this section. In our analysis we make use of those sets of models that have been made available electronically by the authors. We refer the interested reader to the references cited for more detail on individual sets of calculations. We do not attempt to assess the physical validity, triumphs, or shortcomings of the individual models; we present them purely for consideration in comparison with stellar masses fundamentally determined based on astrophysical data.

2.1. *Victoria Group: S93 Models*

The heritage of the Swenson et al. (1994) models resides in the Victoria stellar evolutionary code of VandenBerg (1983, 1992). The notation "S93" refers to a private communication in 1993 of approximately the series F models described in Swenson et al. (1994), provided initially to K. Strom and subsequently to the present authors. The mass range covered is 0.15–5.00 $M_{\odot}$. These models employ the OPAL (Rogers & Iglesias 1992) and Cox & Tabor (1976) opacities, an "improved" Eggleton, Faulkner, & Flannery (1973) equation of state, and Fowler, Caughlan, & Zimmerman (1975) and Caughlan & Fowler (1988) reaction rates, use a mixing-length parameter $\alpha = 1.957$, and assume abundances of $Y = 0.282$ and $Z = 0.019$. Their starting point is defined as $\rho < 0.01$ g cm^{-3}. Atmospheric treatment is presumed gray. A hint provided in VandenBerg & Clem (2003) suggests that more may be coming from this group on pre–main-sequence evolution, including realistic atmospheres, with the most recent description of main-sequence and post–main-sequence evolution appearing in VandenBerg et al. (2000).

2.2. *D'Antona and Mazzitelli: DM94 and DM97 Models*

D'Antona & Mazzitelli (1994) provided tracks covering 0.1–2.5 $M_{\odot}$, using the first substantial improvement to input physics since the 1980s pre–main-sequence evolutionary papers, which utilized 1970s era physics. The models employ the Alexander, Augason, & Johnson (1989) or Kurucz (1991) and Rogers & Iglesias (1992) opacities, the Mihalas, Däppen, & Hummer (1988) and Magni & Mazzitelli (1979) equation of state, and Caughlan & Fowler (1988) and Fowler et al. (1975) reaction rates, use either a mixing-length parameter $\alpha = 1.2$ or the newly introduced Canuto & Mazzitelli (1991, 1992) "full spectrum of turbulence" (FST) convection prescription as a rival to the standard mixing-length theory (MLT), and assume abundances of $Y = 0.285$ and $Z = 0.018$. Atmospheric treatment is gray. Their starting point is the sequence of deuterium burning. These models were updated to cover 0.017–3.00 $M_{\odot}$ in D'Antona & Mazzitelli (1997) and again in 1998 (the later being a "Web-only" correction at less than 0.2 $M_{\odot}$ to the originally circulated 1997 models). As this article went to press we became aware of the Montalbán et al. (2004) calculations, which explore both MLT and FST convection and now use the nongray Hauschildt, Allard, & Baron (1999) or the Heiter et al. (2002), aka Kurucz, atmospheres. These models are not electronically available at present and are not used in our analysis.

2.3. *Geneva Group*

The Charbonnel et al. (1999) models cover 0.4–1.0 $M_\odot$ and represent an extension to lower masses of the Geneva code. They employ the MHD (Hummer & Mihalas 1988; Mihalas et al. 1988; Däppen et al. 1988) equation of state, the Alexander & Ferguson (1994) and Iglesias & Rogers (1996) opacities, Caughlan & Fowler (1988) reaction rates, a mixing-length parameter $\alpha = 1.6$, and abundances of $Y = 0.280$ and $Z = 0.020$. The atmospheric treatment down to $\tau = 2/3$ is gray. These models are not publicly available and are not utilized in the present study.

2.4. *Palla and Stahler: PS99 Models*

The Palla & Stahler (1999) models cover 0.1–6.0 $M_\odot$, use the Rosseland mean opacity, the Eggleton et al. (1973) and Pols et al. (1995) equation of state, Fowler et al. (1975) and Harris et al. (1983) reaction rates, and a mixing-length parameter $\alpha = 1.5$, and assume abundances of $Y = 0.28$ and $Z = 0.02$. The calculations explicitly include a "birth line," or initial mass-radius relationship (which, incidentally, could be adopted and independently applied to any of the other calculations reviewed in this section). Atmospheric treatment is gray. These models do not extend beyond ages of 10^8 yr.

2.5. *Grenoble Group: S00 Models*

The Grenoble group has published their calculations in Forestini (1994), Siess et al. (1997), and, most recently, Siess et al. (2000). The calculations cover 0.1–7.0 $M_\odot$. They use the Alexander & Ferguson (1994) and Iglesias & Rogers (1996) opacities, a modified Pols et al. (1995) scheme for the equation of state, Caughlan & Fowler (1988) reaction rates, a mixing-length parameter $\alpha = 1.6$, and abundances of $Y = 0.288$ and $Z = 0.0189$. These models attempt to include a "realistic" atmosphere as the outer boundary condition, using data from Plez (1992) and Kurucz (1991).

2.6. *Lyon Group: B98 Models*

The Lyon group published models in Baraffe et al. (1995), Chabrier & Baraffe (1997), and Baraffe et al. 1998. The calculations cover 0.035–1.2 $M_\odot$; see Chabrier et al. (2000) and Baraffe et al. (2002) for an extension to 0.001 $M_\odot$. The Lyon group uses the Alexander & Ferguson (1994) and Iglesias & Rogers (1996) opacities, the Saumon, Chabrier, & Van Horn (1995) equation of state, reaction rates described in Chabrier & Baraffe (1997), several different values for the mixing-length parameter, $\alpha = 1.0$, 1.5, and 1.9, and abundances of $Y = 0.275$ and 0.282 and $Z = 0.02$. These models also employ the nongray Hauschildt et al. (1999) atmospheres, which include molecular opacity sources, such as TiO and H_2O, as well as dust grains. It should be noted that the $\alpha = 1.9$ models are actually the same as the $\alpha = 1.0$ ones below 0.6 $M_\odot$ and also that the $\alpha = 1.9$ models actually use $\alpha = 1.0$ in the atmospheres at optical depths of less than 100. The B98 models do not extend to radii larger than those defined by the 10^6 yr isochrone, limiting their utility in studies of young low-mass star-forming regions, where populations are frequently found above the limit of the B98 tracks.

2.7. *Yale Group: Y^2 and YREC Models*

The Yale group has two current sets of models, one called "Y^2" and the other "YREC"; the latter includes rotation.

The Y^2 models cover 0.4–5.0 $M_\odot$ and have been published in a series of papers: Yi et al. (2001, 2003) and Kim et al. (2002). These models use Iglesias & Rogers (1996) and Alexander & Ferguson (1994) opacities, the Cox & Giuli (1968) and Rogers, Swenson, & Iglesias (1996) equation of state with implementation of the Debye-Hückel correction (Guenther et al. 1992), reaction rates from Bahcall & Pinsonneault (1992), a mixing-length parameter $\alpha = 1.7431$, and a range of abundances, from which we have chosen the $X = 0.71$, $Y = 0.27$, $Z = 0.02$ models for comparison. Atmospheres are presumed gray, but for the purpose of calculating colors (not relevant to the present study) are matched in a semiempirical way to the color-temperature relations adopted by Lejeune, Cuisinier, & Buser (1998).[1] These models begin at the theoretically defined deuterium-burning main sequence.

The YREC (Yale Rotating Evolution Code) models cover 0.1–2.25 $M_\odot$ and have been published in Guenther et al. (1992) and Sills, Pinsonneault, & Terndrup (2000). Currently these models also use Iglesias & Rogers (1996) and Alexander & Ferguson (1994) opacities, the Rogers et al. (1996) but also the Saumon et al. (1995) equations of state as appropriate, reaction rates from Gruzinov & Bahcall (1998), a mixing-length parameter $\alpha = 1.72$, and abundances corresponding to $Y = 0.273$ and $Z = 0.0176$ at the age of the Sun. The atmospheric treatment is the same as in the Y^2 models. These models are not publicly available and are not utilized in the present study.

2.8. *Comparison of Models and Systematic Effects*

As illustrated by the above discussion of the gamut of pre–main-sequence evolutionary models, there is substantial variation in the treatment of various aspects of the physics, as well as in the adopted values of certain parameters. The most salient of these differences are in the opacity sources, treatment of convection, and treatment of interior/atmospheric boundary conditions. For comparison between the results of several of the above-mentioned codes at low masses, we show in Figure 1 the predicted contraction tracks for different stellar masses and in Figure 2 the resulting zero-age main sequences (ZAMSs), as defined in § 3.4. Systematic differences are apparent in the mass tracks, especially at young ages, and on the main sequence, particularly at low masses. The variations between tracks are predominantly in temperature and only secondarily in luminosity.

The predicted effective temperature for a given-mass star is dictated largely by the treatment of convection in both the atmosphere and the interior. Because of the extreme complexity of a realistic prescription, convection is usually handled by adopting the mathematically simple MLT (Böhm-Vitense 1958), although more sophisticated prescriptions have been proposed (e.g., Canuto & Mazzitelli 1992). Typically, larger mixing lengths (more efficient convection) predict hotter evolutionary tracks and yield lower masses for a given position in the H-R diagram. The choice of the mixing length is a large uncertainty in current models. A common value is one that predicts 1 $M_\odot$ model agreement with the solar model, but this approach may artificially compensate for other inadequacies in the calculations. For example, several other major aspects of convection can affect the track temperatures, such as how the interior is matched to atmosphere, the thickness of the convective region, and the extent of convective overshooting (see,

[1] We note specifically that the $V-K$ vs. $\log T_{\rm eff}$ relationship given in Lejeune et al. places the M dwarfs in the present study not on the main sequence, but rather substantially warmer and fainter than the main sequence.

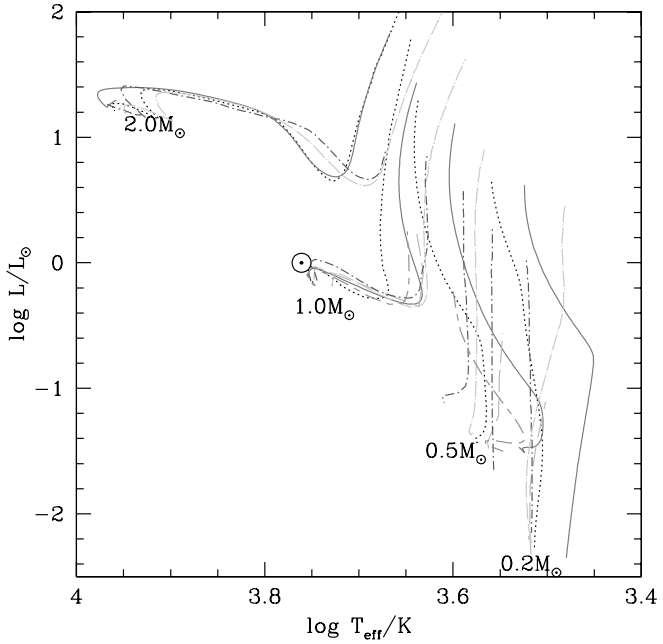

FIG. 1.—Variation between pre–main-sequence contraction tracks for masses 0.2, 0.5, 1.0, and 2.0 $M_\odot$ for the following models: S93 (*solid line*), DM97, with 1998 correction (*dotted line*), B98 $\alpha = 1.9$ (*long-dashed line*), PS99 (*dot–short-dashed line*), S00 (*dot–long-dashed line*), and Y^2 (*long-dash–short-dashed line*). Note that the PS99 models, for which no 0.5 $M_\odot$ track is available, have both the 0.4 and the 0.6 $M_\odot$ tracks plotted instead. Note also that the Y^2 models do not extend as low as 0.2 $M_\odot$. [*See the electronic edition of the Journal for a color version of this figure.*]

e.g., D'Antona & Mazzitelli 1994; Montalbán et al. 2004). Consequently, the treatment of convection is one of the primary uncertainties in current evolutionary models. A related effect is the opacity (including the influence of metallicity) through which the convective energy transport must occur. Higher opacities generally mean lower predicted effective temperatures for a given-mass star.

Another point of comparison between sets of models is the match between the various 1 $M_\odot$ tracks and the location of the Sun. The Sun is evolved from its ZAMS location, having become hotter, larger, and more luminous. In some cases, certain parameters in the above sets of models have been adjusted by the model authors such that their 1 $M_\odot$ model reproduces the temperature and luminosity of the present-day Sun. This requires that the model tracks extend beyond the ZAMS. Nevertheless, we illustrate in Figures 1 and 2 the location of the Sun compared to 1 $M_\odot$ pre–main-sequence tracks and ZAMSs (effectively, the 10^8 yr isochrone at this mass; see § 3.4) from various models. This comparison notwithstanding, we demonstrate in our results that there is little correspondence between models' ability to match the observed main-sequence parameters and the observed pre–main-sequence parameters.

Finally, it should be stressed that there is generally poor agreement between the various models and the empirical main sequence at low masses (Fig. 2). Of note is that the Y^2 models, which at low masses do seem to reach temperatures as cool as in the empirical data, do not display the same downturn at low temperatures as other models. A downturn, such as that displayed by the S93 models in the same cool regime and by the other models at much warmer temperatures, is expected on the basis of the dissociation of H_2 (Copeland, Jensen, & Jørgensen 1970).

3. ASTROPHYSICAL DATA

3.1. *Sample and Selection Criteria*

In order to test the predictions of the various pre–main-sequence evolutionary tracks just discussed, we have compiled from the literature a list of stars with dynamically determined masses and with luminosity and temperature estimates for placing them on the H-R diagram. The sample is restricted to stars less massive than 2.0 $M_\odot$. Of the 148 stars in this sample (Table 1), 88 are main-sequence and 27 are pre–main-sequence stars; the remaining 33 stars are determined to be post–main-sequence, as described below. The Sun is included as a main-sequence star, with stellar parameters adopted from Gray (1992).

For the main-sequence sample, we require masses measured to better than 10%. We strive to exclude W UMa–type contact binaries (e.g., V781 Tau; Liu & Yang 2000), in which tidal effects or mass transfer could be important. Further, to avoid including stars evolved too far beyond the ZAMS, we have retained for analysis only those binary components in Table 1 with $\log g > 4.20$ cm s^{-2}, and thus stars less evolved than $\sim$600 Myr from the ZAMS near our upper mass range and less evolved than 1–3 Gyr from the ZAMS near the solar mass range (according to the Girardi et al. 2000 post-ZAMS models). We begin with the catalog of Andersen (1991) and the additional lists compiled by Ribas et al. (2000), Delfosse et al. (2000), and

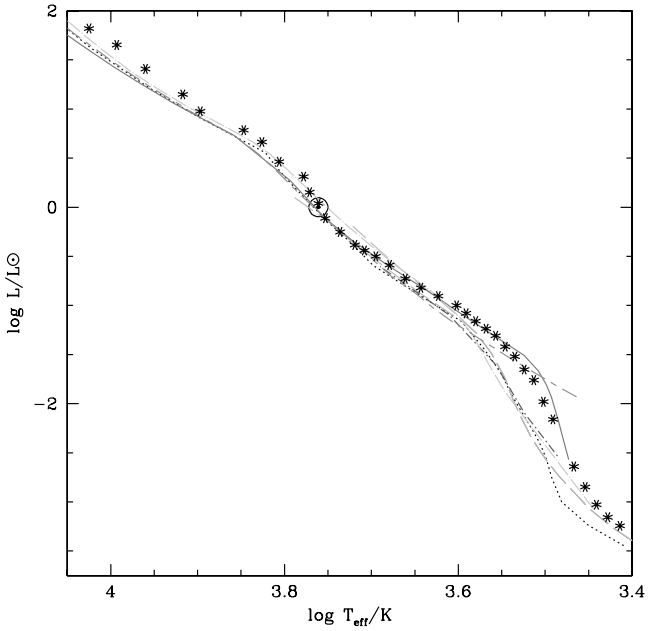

FIG. 2.—Comparison of the composite main sequences adopted here using the various evolutionary models. Line types are as in Fig. 1. Asterisks show the "empirical" main sequence derived from measurements of M_V and our adopted dwarf bolometric correction and temperature scales (see the Appendix). Note that the empirical main sequence represents the average observed luminosity as a function of temperature along the main sequence and not necessarily the ZAMS. Consequently, the highest mass main-sequence stars are, on average, more evolved relative to the zero age than the average solar-mass main-sequence star; this likely causes the apparent overluminous location of the empirical main-sequence at higher masses. The S93 and the Y^2 models reach cool enough temperatures to more accurately reproduce the low-mass empirical main sequence than the other calculations; note, however, the "straight" nature of the Y^2 main sequence, which is at odds with the expected downturn due to H_2 dissociation. [*See the electronic edition of the Journal for a color version of this figure.*]

TABLE 1

SAMPLE AND STELLAR PARAMETERS

NAME	M ($M_\odot$)	R ($R_\odot$)	$\log g$ (cm s^{-2})	TYPE		SPECTRAL TYPE		TEMPERATURE AND LUMINOSITY			EVOLUTIONARY STATUS[c]	COMMENT
				Code[a]	Reference	Type	Reference	$\log T_{\rm eff}$[b]	$\log(L/L_\odot)$	Reference		
Candidate Main-Sequence Stars												
WW Aur A	1.987 ± 0.034	1.883 ± 0.038	4.187 ± 0.019	EB	A91	A5m	A91	3.910 ± 0.015	1.140 ± 0.060	A91	3	
V909 Cyg A	1.980 ± 0.030	1.470 ± 0.020	4.403 ± 0.012	EB	L97c	A0	L97c	3.987 ± 0.021	1.230 ± 0.090	L97c	1	
KW Hya A	1.978 ± 0.036	2.125 ± 0.016	4.079 ± 0.013	EB	A91	A5m	A91	3.900 ± 0.006	1.207 ± 0.025	R00	3	
AI Hya B	1.978 ± 0.036	2.766 ± 0.017	3.850 ± 0.010	EB	A91	F0 V	A91	3.869 ± 0.009	1.312 ± 0.036	R00	3	
V1647 Sgr B	1.972 ± 0.033	1.666 ± 0.017	4.289 ± 0.012	EB	A91	A1 V	A91	3.949 ± 0.014	1.192 ± 0.057	R00	1	
TZ For B	1.949 ± 0.027	3.962 ± 0.088	3.532 ± 0.020	EB	A91	F7 IV	A91	3.803 ± 0.007	1.360 ± 0.030	A91	3	
V624 Her B	1.881 ± 0.013	2.209 ± 0.034	4.024 ± 0.014	EB	A91	A7 V	A91	3.900 ± 0.008	1.240 ± 0.040	A91	3	
MY Cyg B	1.811 ± 0.025	2.193 ± 0.050	4.014 ± 0.021	EB	A91	F0m	A91	3.846 ± 0.010	1.019 ± 0.045	R00	3	
GK Dra B	1.810 ± 0.109	2.830 ± 0.054	3.790 ± 0.041	EB	Z03	...	...	3.837 ± 0.004	1.188 ± 0.029	Z03	3	
51 Tau A	1.800 ± 0.130	...	...	O	T97b	...	...	3.859 ± 0.013	1.046 ± 0.040	T97b	3	Hyades member
WW Aur B	1.799 ± 0.025	1.883 ± 0.038	4.143 ± 0.018	EB	A91	A7m	A91	3.890 ± 0.015	1.060 ± 0.060	A91	3	
V477 Cyg A	1.790 ± 0.120	1.570 ± 0.050	4.300 ± 0.030	EB	GQ92	...	...	3.939 ± 0.015	1.100 ± 0.050	GQ92	1	
V477 Cyg B	1.790 ± 0.120	1.270 ± 0.040	4.360 ± 0.030	EB	GQ92	...	...	3.826 ± 0.015	0.470 ± 0.050	GQ92	1	
MY Cyg A	1.786 ± 0.030	2.193 ± 0.050	4.008 ± 0.021	EB	A91	F0m	A91	3.850 ± 0.010	1.035 ± 0.045	R00	3	
V909 Cyg B	1.750 ± 0.030	1.570 ± 0.030	4.288 ± 0.017	EB	L97c	A2	L97c	3.944 ± 0.016	1.120 ± 0.070	L97c	1	
IQ Per B	1.737 ± 0.031	1.503 ± 0.017	4.323 ± 0.013	EB	A91	A6 V	A91	3.906 ± 0.008	0.930 ± 0.033	R00	1	
OO Peg A	1.720 ± 0.030	2.190 ± 0.080	3.990 ± 0.040	EB	M01	...	...	3.943 ± 0.007	1.388 ± 0.044	M01	3	
OO Peg B	1.690 ± 0.030	1.370 ± 0.050	4.390 ± 0.040	EB	M01	...	...	3.939 ± 0.009	0.964 ± 0.048	M01	1	
V526 Sgr B	1.680 ± 0.060	1.560 ± 0.020	4.280 ± 0.020	EB	L97b	A2	L97b	3.940 ± 0.005	1.100 ± 0.030	L97b	1	
TV Nor B	1.665 ± 0.018	1.550 ± 0.014	4.278 ± 0.012	EB	N97	...	...	3.892 ± 0.006	0.902 ± 0.035	N97	1	
PV Pup A	1.565 ± 0.011	1.542 ± 0.018	4.257 ± 0.010	EB	A91	A8 V	A91	3.840 ± 0.010	0.689 ± 0.041	R00	1	
V442 Cyg A	1.564 ± 0.024	2.072 ± 0.034	3.999 ± 0.016	EB	A91	F1 V	A91	3.839 ± 0.006	0.941 ± 0.028	R00	3	
PV Pup B	1.554 ± 0.013	1.499 ± 0.018	4.278 ± 0.011	EB	A91	A8 V	A91	3.841 ± 0.010	0.668 ± 0.041	R00	1	
RZ Cha A	1.518 ± 0.021	2.264 ± 0.017	3.909 ± 0.009	EB	A91	F5 V	A91	3.816 ± 0.010	0.926 ± 0.041	R00	3	
RZ Cha B	1.509 ± 0.027	2.264 ± 0.017	3.907 ± 0.010	EB	A91	F5 V	A91	3.816 ± 0.010	0.926 ± 0.041	R00	3	
TZ Men B	1.504 ± 0.010	1.432 ± 0.015	4.303 ± 0.009	EB	A91	A8 V	A91	3.857 ± 0.012	0.692 ± 0.049	R00	1	
KW Hya B	1.488 ± 0.017	1.480 ± 0.014	4.270 ± 0.010	EB	A91	F0 V	A91	3.836 ± 0.007	0.637 ± 0.029	R00	1	
BW Aqr A	1.488 ± 0.022	2.064 ± 0.044	3.981 ± 0.020	EB	A91	F7 V	A91	3.800 ± 0.007	0.782 ± 0.034	R00	3	
GK Dra A	1.460 ± 0.066	2.431 ± 0.042	3.830 ± 0.033	EB	Z03	...	...	3.851 ± 0.004	1.112 ± 0.030	Z03	3	
DM Vir A	1.454 ± 0.008	1.763 ± 0.017	4.108 ± 0.009	EB	L96	F7 V	A91	3.806 ± 0.010	0.668 ± 0.041	R00	3	
DM Vir B	1.448 ± 0.008	1.763 ± 0.017	4.106 ± 0.009	EB	L96	F7 V	A91	3.806 ± 0.010	0.668 ± 0.041	R00	3	
CD Tau A	1.442 ± 0.016	1.798 ± 0.017	4.087 ± 0.010	EB	R99	F6 V	R99	3.792 ± 0.004	0.630 ± 0.020	R99	3	
AD Boo A	1.438 ± 0.016	1.614 ± 0.012	4.180 ± 0.011	EB	L97a	...	...	3.805 ± 0.006	0.590 ± 0.030	L97a	3	
V442 Cyg B	1.410 ± 0.023	1.662 ± 0.033	4.146 ± 0.019	EB	A91	F2 V	A91	3.833 ± 0.006	0.726 ± 0.030	R00	3	
V1143 Cyg A	1.391 ± 0.016	1.346 ± 0.023	4.323 ± 0.016	EB	A91	F5 V	A91	3.820 ± 0.008	0.491 ± 0.035	R00	1	
BW Aqr B	1.386 ± 0.021	1.788 ± 0.043	4.075 ± 0.022	EB	A91	F8 V	A91	3.807 ± 0.007	0.685 ± 0.035	R00	3	
CD Tau B	1.368 ± 0.016	1.584 ± 0.020	4.174 ± 0.012	EB	R99	F6 V	R99	3.792 ± 0.004	0.520 ± 0.020	R99	3	
YZ Cas B	1.350 ± 0.010	1.348 ± 0.015	4.309 ± 0.010	EB	A91	F2 V	A91	3.821 ± 0.016	0.496 ± 0.065	R00	1	
V1143 Cyg B	1.347 ± 0.013	1.323 ± 0.023	4.324 ± 0.016	EB	A91	F5 V	A91	3.816 ± 0.008	0.460 ± 0.035	R00	1	
EE Peg B	1.335 ± 0.011	1.312 ± 0.013	4.328 ± 0.009	EB	A91	F5 V	A91	3.802 ± 0.005	0.396 ± 0.022	R00	1	
IT Cas A	1.330 ± 0.009	1.593 ± 0.015	4.158 ± 0.009	EB	L97d	F5 V	L97d	3.811 ± 0.007	0.601 ± 0.035	L97d	3	
IT Cas B	1.328 ± 0.008	1.560 ± 0.040	4.175 ± 0.020	EB	L97d	F5 V	L97d	3.811 ± 0.007	0.583 ± 0.047	L97d	3	
V505 Per A	1.300 ± 0.020	1.400 ± 0.020	4.260 ± 0.010	EB	M01	...	...	3.808 ± 0.003	0.456 ± 0.016	M01	1	
V505 Per B	1.280 ± 0.020	1.140 ± 0.030	4.430 ± 0.010	EB	M01	...	...	3.807 ± 0.004	0.280 ± 0.020	M01	1	

TABLE 1—*Continued*

Name	M ($M_\odot$)	R ($R_\odot$)	$\log g$ (cm s^{-2})	Type		Spectral Type		Temperature and Luminosity			Evolutionary Status[c]	Comment
				Code[a]	Reference	Type	Reference	$\log T_{\rm eff}$[b]	$\log(L/L_\odot)$	Reference		
Candidate Main-Sequence Stars												
V570 Per A	1.280 ± 0.030	1.640 ± 0.160	4.120 ± 0.050	EB	M01	...	...	3.810 ± 0.010	0.600 ± 0.072	M01	3	
HS Hya A	1.2552 ± 0.0078	1.2747 ± 0.0072	4.3259 ± 0.0056	EB	T97a	...	...	3.8129 ± 0.0033	0.415 ± 0.014	T97a	1	
RT And A	1.240 ± 0.030	1.260 ± 0.015	4.335 ± 0.015	EB	P94	F8 V	St93	3.785 ± 0.015	0.290 ± 0.060	P94	1	CABS
UX Men A	1.238 ± 0.006	1.347 ± 0.013	4.272 ± 0.009	EB	A91	F8 V	A91	3.785 ± 0.007	0.351 ± 0.029	R00	1	
AD Boo B	1.237 ± 0.013	1.211 ± 0.018	4.364 ± 0.019	EB	L97a	...	...	3.775 ± 0.007	0.220 ± 0.040	L97a	1	
AI Phe B	1.231 ± 0.005	2.931 ± 0.007	3.593 ± 0.003	EB	M92	F7 V	A91	3.712 ± 0.013	0.730 ± 0.050	M92	3	
FL Lyr A	1.221 ± 0.016	1.282 ± 0.028	4.309 ± 0.020	EB	A91	F8 V	A91	3.789 ± 0.007	0.320 ± 0.030	A91	1	
V570 Per B	1.220 ± 0.030	1.010 ± 0.025	4.550 ± 0.120	EB	M01	...	...	3.793 ± 0.013	0.080 ± 0.176	M01	1	
HS Hya B	1.2186 ± 0.0070	1.2161 ± 0.0071	4.3539 ± 0.0057	EB	T97a	...	...	3.8062 ± 0.0034	0.347 ± 0.015	T97a	1	
UV Leo A	1.210 ± 0.097	0.973 ± 0.024	4.540 ± 0.053	EB	Z03	...	Z03	3.787 ± 0.005	0.060 ± 0.038	Z03	1	
HR 6697A	1.200 ± 0.110	...	...	O	P00	G0 V	Mc95	3.771 ± 0.015	0.211 ± 0.040	Mc95	1	
UX Men B	1.198 ± 0.007	1.274 ± 0.013	4.306 ± 0.009	EB	A91	F8 V	A91	3.781 ± 0.007	0.287 ± 0.029	R00	1	
EW Ori A	1.194 ± 0.014	1.141 ± 0.011	4.401 ± 0.010	EB	A91	G0 V	A91	3.776 ± 0.007	0.171 ± 0.029	R00	1	
AI Phe A	1.190 ± 0.006	1.762 ± 0.007	4.021 ± 0.004	EB	M92	K0 IV	A91	3.800 ± 0.010	0.640 ± 0.040	M92	3	
BH Vir A	1.165 ± 0.008	1.250 ± 0.025	4.340 ± 0.020	EB	P97	...	P97	3.789 ± 0.005	0.280 ± 0.030	R00	1	
α Cen A	1.160 ± 0.031	...	...	O	P00	G2 V	P00	3.761 ± 0.004	0.181 ± 0.017	GD00	1	
EW Ori B	1.158 ± 0.014	1.145 ± 0.011	4.384 ± 0.010	EB	P97	G5 V	A91	3.762 ± 0.007	0.118 ± 0.029	R00	1	
UV Leo B	1.110 ± 0.100	1.216 ± 0.043	4.310 ± 0.055	EB	Z03	...	Z03	3.759 ± 0.004	0.140 ± 0.045	Z03	1	
V432 Aur B	1.060 ± 0.020	2.130 ± 0.140	3.810 ± 0.060	EB	M04	...	...	3.771 ± 0.007	0.708 ± 0.092	M04	3	
UW LMi A	1.060 ± 0.020	1.230 ± 0.050	4.280 ± 0.030	EB	M04	...	...	3.813 ± 0.007	0.368 ± 0.076	M04	1	
V818 Tau A	1.059 ± 0.006	0.900 ± 0.016	4.554 ± 0.016	EB	TR02	G6 V	G85	3.743 ± 0.008	−0.169 ± 0.035	TR02	1	Hyad; CABS
BH Vir B	1.052 ± 0.006	1.140 ± 0.025	4.350 ± 0.020	EB	P97	...	P97	3.750 ± 0.006	0.066 ± 0.031	R00	1	
UW LMi B	1.040 ± 0.020	1.210 ± 0.060	4.290 ± 0.040	EB	M04	...	...	3.813 ± 0.007	0.356 ± 0.080	M04	1	
CN Lyn A	1.040 ± 0.020	1.800 ± 0.210	3.940 ± 0.100	EB	M04	...	...	3.813 ± 0.007	0.704 ± 0.120	M04	3	
CN Lyn B	1.040 ± 0.020	1.800 ± 0.210	3.940 ± 0.100	EB	M04	...	...	3.813 ± 0.007	0.704 ± 0.112	M04	3	
χ Dra A	1.030 ± 0.050	...	...	O	P00	F7 V	T87	3.742 ± 0.015	0.258 ± 0.047	T87	3	
Sun	1.000 ± 0.000	...	...	...	...	G2	...	3.761 ± 0.001	0.000 ± 0.007	G92	1	
V432 Aur A	0.980 ± 0.020	1.390 ± 0.080	4.140 ± 0.06	EB	M04	...	...	3.785 ± 0.007	0.396 ± 0.088	M04	3	
UV Psc A	0.975 ± 0.009	1.110 ± 0.020	4.335 ± 0.016	EB	P97	G4–6 V	St93	3.762 ± 0.007	0.090 ± 0.030	P97	1	CABS
α Cen B	0.970 ± 0.030	...	...	O	P00	K1 V	P00	3.724 ± 0.004	−0.300 ± 0.011	GD00	1	
CG Cyg A	0.940 ± 0.012	0.890 ± 0.013	4.512 ± 0.014	EB	P94	G9.5 V	St93	3.721 ± 0.015	−0.260 ± 0.060	P94	1	CABS
FL Lyr B	0.960 ± 0.012	0.962 ± 0.028	4.454 ± 0.026	EB	A91	G8 V	A91	3.724 ± 0.008	−0.180 ± 0.040	A91	1	
η Cas A	0.950 ± 0.080	...	...	O	F98	G3 V	F98	3.784 ± 0.004	0.099 ± 0.030	F98	1	
RT And B	0.910 ± 0.020	0.900 ± 0.013	4.484 ± 0.015	EB	P94	K0 V	St93	3.675 ± 0.010	−0.435 ± 0.040	P94	1	CABS
HS Aur A	0.900 ± 0.019	1.004 ± 0.024	4.389 ± 0.023	EB	A91	G8 V	A91	3.728 ± 0.006	−0.130 ± 0.030	A91	1	
70 Oph A	0.900 ± 0.074	...	...	O	P00	K0 V	F98	3.726 ± 0.002	−0.296 ± 0.080	F98	1	
81 Cnc A	0.890 ± 0.029	...	...	O	P00	G8 V	Ma96	3.736 ± 0.015	−0.296 ± 0.060	Ma96	1	
HS Aur B	0.879 ± 0.017	0.873 ± 0.024	4.500 ± 0.025	EB	A91	K0 V	A91	3.716 ± 0.006	−0.300 ± 0.030	A91	1	
ξ Boo A	0.860 ± 0.070	...	...	O	F98	G8V	F98	3.744 ± 0.002	−0.272 ± 0.030	F98	1	
81 Cnc B	0.850 ± 0.026	...	...	O	P00	G8V	Ma96	3.736 ± 0.015	−0.313 ± 0.060	Ma96	1	
HD 195987A	0.844 ± 0.018	...	...	O	To02	...	To02	3.716 ± 0.008	−0.228 ± 0.001	To02	1	[Fe/H] = −0.5
CG Cyg B	0.810 ± 0.013	0.840 ± 0.014	4.505 ± 0.016	EB	P94	K3 V	St93	3.674 ± 0.006	−0.510 ± 0.030	P94	1	CABS
HR 6697B	0.800 ± 0.055	...	...	O	P00	K3 V	Mc95	3.679 ± 0.015	−0.788 ± 0.128	Mc95	1	
70 Oph B	0.780 ± 0.040	...	...	O	P00	K5 V	F98	3.638 ± 0.015	−0.848 ± 0.040	F98	1	

TABLE 1—*Continued*

Name	M ($M_\odot$)	R ($R_\odot$)	$\log g$ (cm s^{-2})	Type		Spectral Type		Temperature and Luminosity			Evolutionary Status[c]	Comment
				Code[a]	Reference	Type	Reference	$\log T_{\rm eff}$[b]	$\log(L/L_\odot)$	Reference		
Candidate Main-Sequence Stars												
V818 Tau B	0.760 ± 0.006	0.768 ± 0.010	4.548 ± 0.011	EB	TR02	K6 V	G85	3.645 ± 0.015	−0.775 ± 0.062	TR02	1	Hyad; CABS
UV Psc B	0.760 ± 0.005	0.830 ± 0.030	4.480 ± 0.031	EB	P97	K0–K2 V	St93	3.677 ± 0.007	−0.500 ± 0.040	P97	1	CABS
χ Dra B	0.730 ± 0.024	...	...	O	P00	K0 V	T87	3.719 ± 0.030	−0.468 ± 0.105	T87	1	
Gl 702B	0.713 ± 0.029	...	...	O	D00	...	...	3.626 ± 0.0119*	−0.805 ± 0.05	D00	1	
ξ Boo B	0.700 ± 0.050	...	...	O	F98	K4 V	F98	3.638 ± 0.015	−1.052 ± 0.080	F98	1	
HD 195987B	0.665 ± 0.008	...	...	O	To02	...	To02	3.623 ± 0.021	−0.949 ± 0.076	To02	1	[Fe/H] = −0.5
η Cas B	0.620 ± 0.060	...	...	O	F98	K7 V	F98	3.606 ± 0.016	−1.157 ± 0.080	F98	1	
YY Gem B	0.601 ± 0.005	0.619 ± 0.006	4.632 ± 0.008	EB	TR02	dM1e	St93	3.582 ± 0.011	−1.135 ± 0.009	TR02	1	CABS
YY Gem A	0.598 ± 0.005	0.619 ± 0.006	4.632 ± 0.008	EB	TR02	dM1e	St93	3.582 ± 0.011	−1.135 ± 0.009	TR02	1	CABS
Gl 570B	0.566 ± 0.003	...	...	O	D00	...	...	3.548 ± 0.0056*	−1.276 ± 0.05	D00	1	
CU Cnc Aa	0.433 ± 0.002	0.432 ± 0.005	4.804 ± 0.011	EB	R03	M3.5 V	R03	3.500 ± 0.021	−1.778 ± 0.083	R03	1	
Gl 644A	0.4155 ± 0.0057	...	...	O	Se00	...	...	3.524 ± 0.0036*	−1.674 ± 0.05	D00	1	
CU Cnc Ab	0.398 ± 0.001	0.391 ± 0.009	4.854 ± 0.021	EB	R03	M3.5 V	R03	3.495 ± 0.021	−1.884 ± 0.086	R03	1	
Gl 661A	0.379 ± 0.035	...	...	A	D00	...	...	3.509 ± 0.0028*	−1.695 ± 0.05	D00	1	
Gl 570C	0.377 ± 0.002	...	...	O	D00	...	...	3.519 ± 0.0083*	−1.768 ± 0.05	D00	1	
Gl 661B	0.369 ± 0.035	...	...	A	D00	...	...	3.526 ± 0.0039*	−1.843 ± 0.05	D00	1	
Gl 623A	0.343 ± 0.011	...	...	O	D00	...	...	3.531 ± 0.0032*	−1.707 ± 0.05	D00	1	
Gl 831A	0.291 ± 0.013	...	...	O	Se00	...	...	3.486 ± 0.0022*	−2.014 ± 0.05	D00	1	
Gl 860A	0.271 ± 0.010	...	...	O	D00	...	...	3.507 ± 0.0023*	−1.936 ± 0.05	D00	1	
CM Dra A	0.2307 ± 0.0010	0.252 ± 0.002	4.998 ± 0.002	EB	Me96	M4 Ve	St93	3.488 ± 0.008	−2.301 ± 0.044	V97	1	
CM Dra B	0.2136 ± 0.0010	0.235 ± 0.002	5.025 ± 0.007	EB	Me96	M4 Ve	St93	3.488 ± 0.008	−2.360 ± 0.044	V97	1	
Gl 747A	0.2137 ± 0.0009	...	...	O	Se00	...	...	3.508 ± 0.0026*	−2.165 ± 0.05	D00	1	
Gl 234A	0.2027 ± 0.0106	...	...	O	Se00	...	...	3.486 ± 0.0018*	−2.237 ± 0.05	D00	1	
Gl 747B	0.1997 ± 0.0008	...	...	O	Se00	...	...	3.504 ± 0.0026*	−2.213 ± 0.05	D00	1	
Gl 860B	0.176 ± 0.007	...	...	O	D00	...	...	3.495 ± 0.0040*	−2.497 ± 0.05	D00	1	
Gl 831B	0.1621 ± 0.0065	...	...	O	Se00	...	...	3.463 ± 0.0022*	−2.562 ± 0.05	D00	1	
Gl 473A	0.143 ± 0.011	...	...	A	T99	...	...	3.455 ± 0.0021*	−2.607 ± 0.05	D00	1	
Gl 473B	0.131 ± 0.010	...	...	A	T99	...	...	3.466 ± 0.0026*	−2.745 ± 0.05	D00	1	
Gl 866B	0.1145 ± 0.0012	...	...	O	Se00	...	...	3.453 ± 0.0021*	−2.837 ± 0.05	D00	1	
Gl 623B	0.114 ± 0.008	...	...	A	D00	...	...	3.453 ± 0.0042*	−2.986 ± 0.05	D00	1	
Gl 234B	0.1034 ± 0.0035	...	...	O	D00	...	...	3.448 ± 0.0019*	−2.977 ± 0.05	D00	1	
Gl 65A	0.102 ± 0.010	...	...	A	D00	...	...	3.454 ± 0.0020*	−2.754 ± 0.05	D00	1	
Gl 65B	0.100 ± 0.010	...	...	A	D00	...	...	3.453 ± 0.0022*	−2.920 ± 0.05	D00	1	
Pre–Main-Sequence Stars												
RS Cha A	1.858 ± 0.016	2.137 ± 0.055	4.047 ± 0.023	EB	A91	A8	M00	3.883 ± 0.010	1.144 ± 0.044	M00	2	
RS Cha B	1.821 ± 0.018	2.338 ± 0.055	3.961 ± 0.021	EB	A91	A8	M00	3.859 ± 0.010	1.126 ± 0.043	M00	2	
MWC 480	1.650 ± 0.070	...	...	D	Si00	A2–3	JJA88	3.948 ± 0.015*	1.243 ± 0.10	...	2	
TY CrA B	1.640 ± 0.010	2.080 ± 0.140	4.020 ± 0.050	EB	C98	...	C98	3.690 ± 0.035	0.380 ± 0.145	C98	2	
045251+3016A	1.450 ± 0.190	...	...	O	St01	K5	St01	3.643 ± 0.015*	−0.167 ± 0.053	St01	2	
AK Sco A	1.350 ± 0.070	1.590 ± 0.350	...	SB	A03	F5	A89	3.813 ± 0.007	0.607 ± 0.050	A03	2	
AK Sco B	1.350 ± 0.070	1.590 ± 0.350	...	SB	A03	F5	A89	3.813 ± 0.007	0.607 ± 0.050	A03	2	
BP Tau	1.320 ± 0.200	...	...	D	Du03	K7	B90, H95	3.608 ± 0.012	−0.780 ± 0.10	JVK99	2	

TABLE 1—*Continued*

Name	M ($M_\odot$)	R ($R_\odot$)	$\log g$ (cm s^{-2})	Type		Spectral Type		Temperature and Luminosity			Evolutionary Status[c]	Comment
				Code[a]	Reference	Type	Reference	$\log T_{\rm eff}$[b]	$\log(L/L_\odot)$	Reference		
Pre–Main-Sequence Stars												
0529.4+0041A	1.250 ± 0.050	1.700 ± 0.200	4.070 ± 0.100	EB	C00	K1–K2	C00	3.701 ± 0.009	0.243 ± 0.037	C00	2	
EK Cep B	1.124 ± 0.012	1.320 ± 0.015	4.250 ± 0.015	EB	P87	...	...	3.755 ± 0.015	0.190 ± 0.070	P87	2	
UZ Tau Aa	1.016 ± 0.065	...	...	DSB	Si00	M1	P02	3.557 ± 0.015*	−0.201 ± 0.124	P02	2	
V1174 Ori A	1.009 ± 0.015	1.339 ± 0.015	4.19 ± 0.01	EB	S04	K4.5	S04	3.650 ± 0.011*	−0.193 ± 0.048	S04	2	
0529.4+0041B	0.910 ± 0.050	1.200 ± 0.200	4.240 ± 0.150	EB	C00	K7–M0	C00	3.604 ± 0.022	−0.469 ± 0.192	C00	2	
LkCa 15	0.970 ± 0.030	...	...	D	Si00	K5	H86	3.643 ± 0.015*	−0.165 ± 0.10	...	2	
GM Aur	0.840 ± 0.050	...	...	D	Si00	K7	B90, H95	3.602 ± 0.015*	0.598 ± 0.10	...	2	
045251+3016B	0.810 ± 0.090	...	...	O	St01	...	...	3.535 ± 0.015*	−0.830 ± 0.086	St01	2	
V1174 Ori B	0.731 ± 0.008	1.065 ± 0.011	4.25 ± 0.01	EB	S04	M1.5	S04	3.558 ± 0.011	−0.761 ± 0.058	S04	2	
DL Tau	0.720 ± 0.110	...	...	D	Si00	K7–M0	B90, H95	3.591 ± 0.015*	0.005 ± 0.10	...	2	
DM Tau	0.550 ± 0.030	...	...	D	Si00	M1	V93	3.557 ± 0.015*	−0.532 ± 0.10	...	2	
CY Tau	0.550 ± 0.330	...	...	D	Si00	M2	SS94	3.535 ± 0.015*	−0.491 ± 0.10	...	2	
UZ Tau Ab	0.294 ± 0.027	...	...	DSB	Si00	M4	P02	3.491 ± 0.015*	−0.553 ± 0.124	P02	2	
Pre–Main-Sequence Composite Systems												
GG Tau Aa	(1.28 ± 0.07)C	...	...	D	Si01	M0	HK03	3.580 ± 0.015*	−0.106 ± 0.10	...	2	
GG Tau Ab	(1.28 ± 0.07)(1 − C)	...	...	D	Si01	M2	HK03	3.535 ± 0.015*	−0.338 ± 0.10	...	2	
DF Tau A	(0.90 ± 0.60)C	...	...	A	S03	M2	HK03	3.535 ± 0.015*	−0.255 ± 0.10	...	2	
DF Tau B	(0.90 ± 0.60)(1 − C)	...	...	A	S03	M2.5	HK03	3.524 ± 0.015*	−0.162 ± 0.10	...	2	
FS Tau A	(0.78 ± 0.25)C	...	...	A	Ta02	M0	HK03	3.580 ± 0.015*	−1.293 ± 0.10	...	2	
FS Tau B	(0.78 ± 0.25)(1 − C)	...	...	A	Ta02	M3.5	HK03	3.502 ± 0.015*	−1.552 ± 0.10	...	2	
FO Tau A	(0.77 ± 0.25)C	...	...	A	Ta02	M3.5	HK03	3.502 ± 0.015*	−0.581 ± 0.10	...	2	
FO Tau B	(0.77 ± 0.25)(1 − C)	...	...	A	Ta02	M3.5	HK03	3.502 ± 0.015*	−0.609 ± 0.10	...	2	

Note.—Table 1 is also available in machine-readable form in the electronic edition of the Astrophysical Journal.

[a] Method used to determine the dynamical mass: (EB) eclipsing binary system; (O) astrometric + radial velocity orbit; (A) astrometric orbit + distance estimate; (D) disk kinematics; (DSB) disk kinematics + doubled-lined spectroscopic binary.

[b] Main-sequence temperatures with asterisks are determined from colors; pre–main-sequence temperatures with asterisks are determined from a spectral type.

[c] Evolutionary status code: (1) main sequence; (2) pre–main sequence; (3) post–main sequence/evolved.

References.—(A91) Andersen 1991; (A03) Alencar et al. 2003; (A89) Andersen et al. 1989; (B90) Basri & Batalha 1990; (C98) Casey et al. 1998; (C00) Covino et al. 2000; (D00) Delfosse et al. 2000; (Du03) Dutrey et al. 2003; (F98) Fernandes et al. 1998; (G85) Griffin 1985; (G92) Gray 1992; (GD00) Guenther & Demarque 2000; (GQ92) Giménez & Quintana 1992; (H86) Herbig, Vrba, & Rydgren 1986; (H95) Hartigan, Edwards, & Ghandour 1995; (HK03) Hartigan & Kenyon 2003; (JJA88) Jaschek, Jaschek, & Andrillat 1988; (JVK99) Johns-Krull et al. 1999; (L96) Latham et al. 1996; (L97a) Lacy 1997a; (L97b) Lacy 1997b; (L97c) Lacy 1997c; (L97d) Lacy et al. 1997; (Ma96) Mason, McAlister, & Hartkopf 1996; (Mc95) McAlister et al. 1995; (Me96) Metcalfe et al.1996; (M00) Mamajek, Lawson, & Feigelson 2000; (M01) Munari et al. 2001; (M04) Marrese et al. 2004; (M92) Milone, Stagg, & Kurucz 1992; (N97) North, Studer, & Künzli 1997; (P87) Popper 1987; (P94) Popper 1994; (P97) Popper 1997; (P00) Pourbaix 2000; (P02) Prato et al. 2002; (R99) Ribas, Jordi, & Torra 1999; (R00) Ribas et al. 2000; (R03) Ribas 2003; (Se00) Ségransan et al. 2000; (Si00) Simon et al. 2000; (St01) Steffen et al. 2001; (SS94) Stüwe & Schulz 1994; (S03) Schaefer et al. 2003; (St93) Strassmeier et al. 1993; (S04) Stassun et al. (2004); (Ta02) Tamazian et al. 2002; (T87) Tomkin et al. 1987; (T97a) Torres et al. 1997a; (T97b) Torres, Stefanik, & Latham 1997b; (T99) Torres et al. 1999; (TR02) Torres & Ribas 2002; (To02) Torres et al. 2002; (V93) Valenti, Basri, & Johns 1993; (V97) Viti et al. 1997; (Z03) Zwitter et al. 2003.

Lastennet & Valls-Gabaud (2002), but also include systems more recently identified in Munari et al. (2001), Zwitter et al. (2003), and Marrese et al. (2004). Of the compiled systems surviving our selection criteria, most are detached double-lined eclipsing binaries. The remaining main-sequence stars are spatially resolved double-lined spectroscopic binaries that have independent temperature estimates for each component from spectroscopic or color measurements that enable their placement on the H-R diagram. We note that the main-sequence sample of stars suitable for our purposes has, historically, been biased toward solar or greater masses. In recent years, however, the sample of stars at masses of less than 0.5 $M_{\odot}$ with both dynamical masses and independent temperature and luminosity estimates for the two components has grown considerably (e.g., Delfosse et al. 2000).

The pre–main-sequence sample is not subjected to the same dynamical mass uncertainty restriction that is applied to the main-sequence sample ($\sigma < 10\%$), because of the small numbers of stars having measured masses. These 27 pre–main-sequence stars include eight components of double-lined eclipsing binary systems (TY Cr Ab, EK Cep B, RS Cha A and B, RX J0529.4+0041A and B, and AK Sco A and B; see references in Table 1), which have the most accurately determined masses among the pre–main-sequence sample ($\sigma \leq 5\%$) but are all approximately solar or larger mass stars. One pre–main-sequence system has component masses determined from spatially resolved measurements of a double-lined spectroscopic binary (NTTS 045251+30016A and B; Steffen et al. 2001). Nine pre–main-sequence stars have masses determined from disk kinematics (Simon et al. 2000; Dutrey et al. 2003). In the case of the UZ Tau E binary, the component masses are determined from the spectroscopic orbit inferred by Prato et al. (2002). The remaining pre–main-sequence systems (FO Tau, FS Tau, DF Tau, and GG Tau) are all binaries that have only total dynamical mass estimates; in these cases, we thus compare these total dynamical masses with the summed masses inferred from placement of the individual components on the H-R diagram. Although other pre–main-sequence binary systems have orbital mass estimates, we include only those that have spatially resolved temperature or spectral type measurements. We do not include systems with only mass ratios available.

3.2. *Stellar Parameters I: Mass, Radius, and Surface Gravity*

The sample is listed in Table 1 in order of the most to the least massive star and with pre–main-sequence stars distinguished from main-sequence stars. The mass and radius ranges occupied by the unevolved members of our sample ($\log g > 4.20$ cm s^{-2} for non–pre–main-sequence stars) are shown in Figure 3. For stars that are members of eclipsing systems, radii are determined directly from observations; for the remainder, this quantity has been estimated for plotting purposes from temperature and luminosity following Stefan's Law ($L = 4\pi R^2 \sigma T_{\rm eff}^4$). In the remainder of this section we describe how the masses, radii, and gravities listed in Table 1 were derived by the original authors.

For the double-lined eclipsing binaries, the ratio of velocity amplitudes is inversely proportional to the ratio of masses, while the sum of velocity amplitudes is related via the period to the sum of the masses. Given two equations and two unknowns, the individual component masses can be determined directly from the observables v_1, v_2, and the orbital period. Photometric measurements of the eclipse provide the ratio of radius to semimajor axis, while the assumption of $\approx 90^{\circ}$ system inclination means that radial velocity measurements yield the semimajor axis uniquely, and hence one can solve for the radius directly from the observations (e.g., Covino et al. 2000). Double-lined eclipsing binary systems are the only binary systems with radius estimates determined directly from observables. The radii, combined with the masses, yield surface gravities ($g = GM/R^2$). Only those radii and surface gravities determined from fundamental observables are listed in Table 1.

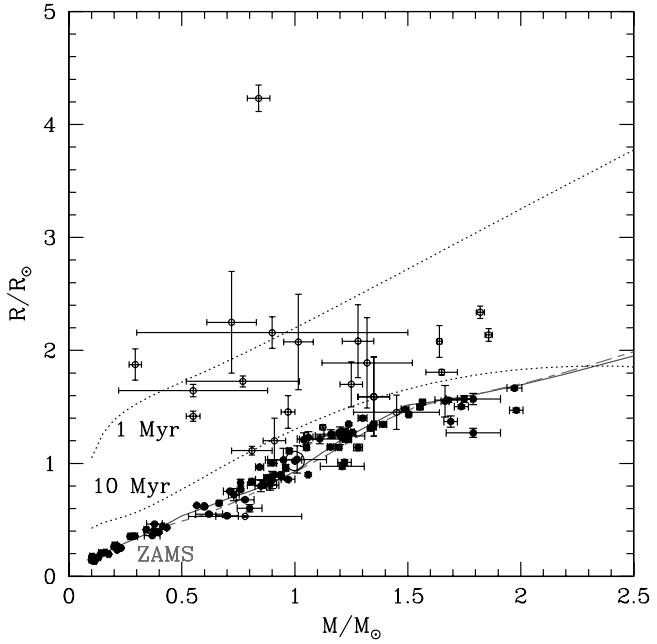

FIG. 3.—Mass and radius measurements for our sample stars. Open symbols represent pre–main-sequence objects and filled symbols main-sequence stars. For the double-lined eclipsing systems both axes are fundamentally derived from observation, whereas for the noneclipsing systems the masses are fundamental, but the radii are inferred from luminosity and effective temperature values in Table 1. The 1 and 10 Myr isochrones of DM97 are indicated (*dotted lines*) to show the approximate change in radius with age as pre–main-sequence stars contract, as are the ZAMSs from S93 (*solid line*) and Y^2 (*dashed line*) models that most closely approximate the empirical main sequence in Fig. 2. [*See the electronic edition of the Journal for a color version of this figure.*]

For the spatially resolved double-lined systems, one does not have the benefit of knowing the system inclination. Instead, one can constrain the inclination via a combined astrometric and radial velocity orbital solution, allowing the individual masses to be recovered (e.g., Steffen et al. 2001). For spatially resolved binaries with an astrometric orbital solution but no radial velocity orbital solution, a total system mass can be determined if a distance is assumed (e.g., Schaefer et al. 2003). Finally, for stars surrounded by spatially resolvable circumstellar gas disks, interferometric measurements that map the velocity profile can be used to dynamically determine the central mass, under the assumption of Keplerian motion (e.g., Simon et al. 2000). In some cases, the central mass may be a binary star.

3.3. *Stellar Parameters II: Temperature and Luminosity*

Comparison of the dynamically determined masses discussed above with those inferred from theoretical calculations requires temperature and luminosity information for every star. In determining these values, we apply the same methods to both the main-sequence and the pre–main-sequence samples. For

the eclipsing binary systems, the ratio of the stellar temperatures is typically determined very precisely from light-curve analysis (see individual references cited in Table 1). These values are then combined with a mean system temperature, estimated from photometrically calibrated atmospheric models (see, e.g., Ribas et al. 2000), to determine individual effective temperatures.[2] Although the temperatures listed in Table 1 are all taken directly from the references and thus in many cases are determined in a nonuniform fashion, we have in all cases adopted the values that use the most recent and accurate photometric calibrations. Since the stellar radius is also a quantity inferred from light-curve analysis, luminosities are then determined directly from Stefan's law and are, for the most part, distance-independent. In some cases, we transformed quoted $M_{\rm bol}$ values to $\log L$ values. We assume $M_{\rm bol,\odot} = 4.75$ mag in all calculations (Cox 2000; see also footnote 7 in VandenBerg et al. 2000).

For the remaining (non–double-lined eclipsing) main-sequence stars, we determine temperatures in one of three ways. Preferably, we adopt temperatures and uncertainties from the listed references when they are determined from a line ratio analysis (e.g., Gray 1994). Alternatively, we estimate the temperatures from the spectral types, or if no spectroscopic information is available, we determine the temperature from the observed photometric colors. We use the temperature–spectral type–color relations described in the Appendix and assume an uncertainty in $\log T$ of 0.015 dex, which corresponds to roughly 1 spectral subclass, even though the formal errors in $\log T$ based on color errors would be substantially smaller. Temperatures determined from either spectral types or colors are noted in Table 1, as they are not fundamental temperature measurements. Luminosities are recalculated here based on optical or infrared photometry, bolometric corrections from the Appendix, and distance estimates. All of the main-sequence stars have parallax information and hence distances. Although the luminosities are recalculated to ensure no systematic errors from different assumptions, we generally adopt the published luminosity uncertainties. For the stars with only spatially resolved photometry, we adopt a uniform uncertainty in $\log L$ of 0.05 dex.

For the remaining (non–double-lined eclipsing) pre–main-sequence stars, temperatures are determined from spectral synthesis, in the case of BP Tau (Johns-Krull, Valenti, & Koresko 1999), or from spectral types and the temperature relation described in the Appendix, assuming an uncertainty of 0.015 dex. Photometric colors alone are insufficient for estimating the temperatures of pre–main-sequence stars, because of possible extinction and continuum excesses from either an accretion shock or the inner circumstellar disk. The luminosities are calculated from $I_{\rm C}$-band measurements, which are the least likely to be contaminated by possible continuum excesses, and are at an optimal wavelength from which to apply a bolometric correction for early A through mid-M spectral types. All pre–main-sequence stars for which we have calculated luminosities are in Taurus; we assume a distance of 140 pc (Kenyon, Dobrzycka, & Hartmann 1994). Also for this subsample of young T Tauri stars, we assume a uniform uncertainty of 0.10 dex in $\log L$, which incorporates typical 1 spectral subclass errors propagated to errors in intrinsic colors and in bolometric corrections used to calculate reddening-free luminosities.

[2] Several eclipsing systems are known to be chromospherically active binary stars (e.g., Strassmeier et al. 1993), in which starspots are an unaccounted-for bias in the temperature estimates. These systems are noted as such ("CABS") in Table 1.

3.4. *Masses Estimated from Tracks*

We derive track-predicted masses for our sample by interpolating between tabulated luminosity and effective temperature values as a function of stellar mass and age for each set of tracks we test. In practice, the methods adopted to determine masses for the main-sequence and pre–main-sequence stars differ slightly. For the pre–main-sequence stars, isochrones are generated at logarithmic ages intermediate to those tabulated by the model authors. The mass is determined via interpolation along the isochrone that intersects the stellar luminosity and temperature. For stars with luminosities that put them above the youngest isochrone, the mass is assigned using this youngest isochrone and the temperature. This occurs only for the B98 tracks and only for a few late K- and M-type T Tauri stars. Uncertainties in the track-predicted masses are determined from the range of masses predicted by varying the luminosity and temperature estimates by their uncertainties, as listed in Table 1.

For stars already on the main sequence, where isochrones converge in the luminosity–effective temperature plane, we have created a theoretical young main sequence for each set of tracks by adopting the 10^8 yr isochrone at masses of 0.7 $M_\odot$ and above (such that stars have already arrived at their ZAMS position but have not yet begun any substantial evolution away from it) and the 10^9 yr isochrone below this mass. Only objects less massive than 0.09 $M_\odot$ have not reached the ZAMS by 10^9 yr, according to the models; the least massive main-sequence star in our sample is 0.10 $M_\odot$. We refer to Figure 2 for comparison of the luminosity–effective temperature relationships adopted as the main sequence for the various sets of tracks. These constructed main sequences represent a unique mass-temperature and mass-luminosity relation for each model. We use these relations to determine the main-sequence masses by averaging, for each star, the mass determined from interpolation of the stellar temperature and that from interpolation of the stellar luminosity. Uncertainties are estimated from the uncertainties in the stellar properties (luminosity and temperature) and the difference between the luminosity- and temperature-predicted masses. This procedure could not be followed for the PS99 tracks, since no 10^9 yr isochrone exists and the 10^8 yr isochrone exists only in the mass range 0.1–0.8 $M_\odot$; no main-sequence masses are determined from these models.

The validity of our adopted main-sequence isochrone merits some discussion. Since there is continuous luminosity and temperature evolution even when stars are on the main sequence, our derived masses are appropriate, in a strict sense, only for the specific age assumed in creating the mass-luminosity or mass-temperature relationships. For example, at masses above 0.7 $M_\odot$, where we have adopted the relationships for 10^8 yr, a 1.0 $M_\odot$ star will have its mass overestimated by 2% if it is really 10^9 yr old, while a 2.0 $M_\odot$ star will have its mass overestimated by 10%. One might think about assuming, for all stars in our main-sequence sample, the mean age in the solar neighborhood of $\sim$3 Gyr. This approach would be incorrect, however, since we have selected stars via their surface gravity to be on the hydrogen-burning main sequence, which corresponds to different mean ages at different masses. If a star is really 3×10^9 yr old, it will not be in our main-sequence sample at 2.0 $M_\odot$, but at 1.0 $M_\odot$ it will have its mass overestimated by 6%. Without precise knowledge of the ages of the stars in our sample, we can only bear these biases in mind;

we cannot correct for them. Because the hydrogen-burning main sequence is widest for the most massive (>10 $M_\odot$) stars and decreases in width toward lower masses, this effect should not limit the conclusions drawn from our primarily low-mass sample.

4. COMPARISON OF TRACK-PREDICTED AND DYNAMICAL MASSES

Figure 4 shows comparisons between the dynamically determined masses and the masses inferred from all eight sets of evolutionary tracks; both the direct correlation of mass and the difference between the two masses as a percentage of the dynamical mass are provided. Figure 5 shows the mean percentage differences between track-predicted and dynamical masses as a function of dynamically determined mass (essentially a binned version of the top plot in each panel of Fig. 4). The standard deviations of the means are plotted as error bars for statistical assessment. In both of these figures the main-sequence and the pre–main-sequence samples are distinguished. The binary systems that have only total system dynamical masses (FO Tau AB, FS Tau AB, DF Tau AB, GG Tau Aa and Ab) have been plotted assuming that the average mass per star is $\frac{1}{2}$ the total dynamical mass and that the average offset per star is $\frac{1}{2}$ the total system difference. This assumption is justified by the similar spectral types of the components of these binaries (Table 1). Figures 4 and 5 illustrate the differences between the predictions of the various pre–main-sequence evolutionary calculations and are now used to assess the robustness of the predicted stellar masses.

4.1. *Main-Sequence Stars*

We first consider the comparison in the main-sequence sample. For the five tracks that extend to the largest masses considered here, 1.2–2.0 $M_\odot$ (S93, DM94, DM97, S00, Y^2), there is excellent agreement between the theoretical and dynamically determined masses in all cases. Closer to 1.0 $M_\odot$, the S93, DM94, DM97, and Y^2 models again predict main-sequence masses that are consistent with dynamically determined values. However, both B98 models and the S00 models predict masses that are 5% (at 1–2 σ) larger than the dynamical masses. This could be an evolutionary effect, since the average age of the solar mass main-sequence stars in our sample is likely more than 10^8 yr. Note, however, that the Sun (Fig. 4, *solar symbol*) resides just beyond the 1 σ error in the mean difference, likely indicating that the Sun is slightly older than the mean 1 $M_\odot$ star in our sample; as discussed in § 3.4, the 10^8 yr isochrone will overestimate the mass of the Sun by 6%, roughly the magnitude of the observed offset. At subsolar masses, all tracks except for S93 and Y^2 predict masses that are less than the dynamically determined values by 15%–30%, at several σ significance. The Y^2 models show the flattest overall trend (see Fig. 5), with agreement between predicted and dynamically determined masses to within 1%–3% over all masses down to 0.6 $M_\odot$; the agreement slips to 7% for the lowest considered mass of 0.4 $M_\odot$. The S93 models, in contrast to other models at low masses, are consistent with dynamical masses down to 0.3 $M_\odot$ but systematically *overpredict* (as opposed to underpredict) the lower masses. Near 0.1 $M_\odot$ (the two lowest mass bins), all models that extend this low appear to reverse their offset trends and again predict masses that are consistent with the dynamically inferred values.

The systematic discrepancy of predicted and dynamical masses for 0.2–0.5 $M_\odot$ main-sequence stars likely stems from the poor match of model 10^9 yr isochrones (our adopted main sequence over this mass range) with the empirical main sequence, as shown in Figure 2. We note that this empirical main sequence is consistent with the location of low-mass main-sequence members of our sample (Fig. 3), confirming that these stars are not peculiar because of, for example, chromospheric activity. The DM97, B98, and S00 models, which all underpredict low-mass stellar masses, are either too hot by ~200 K or underluminous by a factor of 3. We note, however, that masses determined via interpolation of stellar luminosity are more consistent with dynamically determined values than the masses determined via interpolation of stellar temperature (the values adopted for comparison with dynamical masses are the average of the luminosity- and temperature-predicted masses; see § 3.4). This suggests that the main source of discrepancy in the models is the temperature predictions and not the luminosity predictions.

A major cause of systematic disagreement between low-mass dynamical masses and track-predicted masses is disparity between observation and theory in the "break" in the mass-luminosity relationship (seen in the figures as a break in the temperature-luminosity relationship). In most models this break occurs at a temperature hotter ($\log T \sim 3.7$ dex; M0.5 spectral type) than the location of the empirical break ($\log T \sim 3.5$ dex; M3.5 spectral type). Even the Y^2 models, which predict the most consistent masses, are clearly diverging from the empirical main sequence over this mass range; these models exhibit no break in their mass-luminosity (temperature-luminosity) relationship. Only the S93 models offer reasonable agreement with the empirical main sequence at low masses. Interestingly, the standard deviation of the mean offset is much larger at low masses for the S93 models than for other models; this is because the data scatter uniformly around this main sequence, whereas for other models the offset between the data and the predicted main sequence is large, and the standard deviation in the mean offset is substantially smaller, since *all* the data are offset in the same direction and by roughly the same amount. Similar conclusions regarding the accuracy of the predicted main sequence can be derived by comparing open cluster loci to these models (e.g., Stauffer et al. 1995; L. A. Hillenbrand et al. 2004, in preparation). At high masses, the divergence seen in Figure 2 between the models and the empirical main sequence is expected, since most main-sequence stars (i.e., those used to derive the absolute and bolometric magnitudes of typical main-sequence stars) are slightly more evolved than the theoretical ZAMS.

4.2. *Pre–Main-Sequence Stars*

We now consider the pre–main-sequence sample. Relative to our main-sequence sample, these stars have poorly constrained temperatures and luminosities, leading to larger errors in H-R diagram placement and hence larger errors in predicted masses. In addition, the errors in the dynamical masses for this sample are often substantially larger than the 10% limit we imposed on those in the main-sequence sample. Finally, the statistics for the pre–main sequence are comparatively worse, given the small number of pre–main-sequence stars with dynamically determined masses. With these caveats in mind, we interpret the comparisons shown in Figures 4 and 5 with the aid of Figure 6, which shows the results for individual stars, similarly to the top plot in each panel of Figure 4, but with an expanded scale and now with individual error bars.

Above 1.2 $M_\odot$, all models considered (except both B98 calculations, which do not extend above this mass) predict

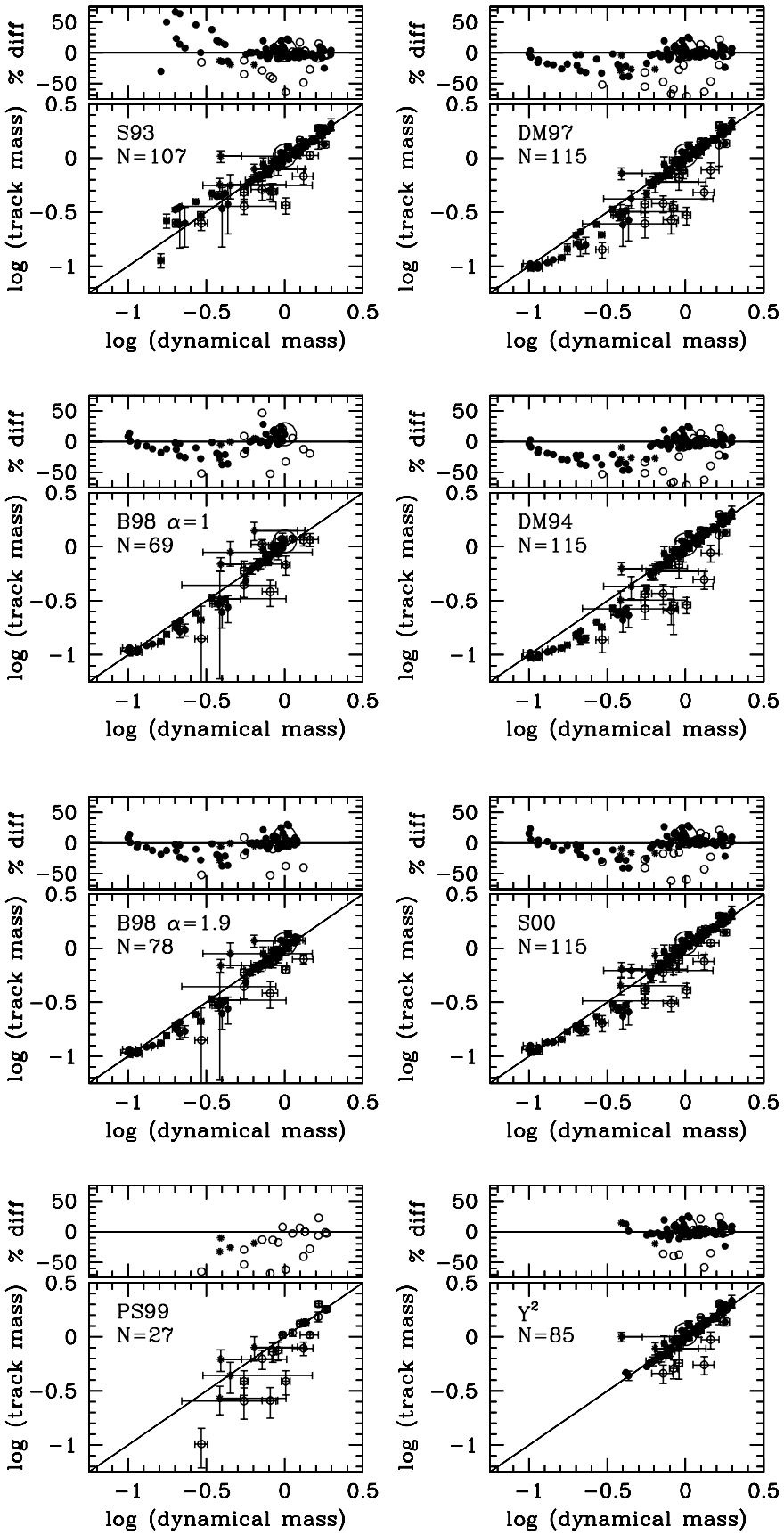

FIG. 4.—Comparison of dynamically determined with track-predicted masses in units of solar masses for main-sequence (*filled symbols*) and pre–main-sequence (*open symbols*) stars. Asterisks represent pre–main-sequence binary systems whose individual components can be placed in the H-R diagram but whose measured dynamical mass is that of the composite system; these systems have been plotted assuming an average dynamical mass of $\frac{1}{2}$ the total dynamical mass and an average percentage mass difference of $\frac{1}{2}$ the total. The Sun is also shown as a large solar symbol. Not all stars in Table 1 appear in all panels, because of the variation between model calculations in the range of masses covered. The percentage mass difference in the top plot in each panel is the track-predicted mass minus dynamical mass.

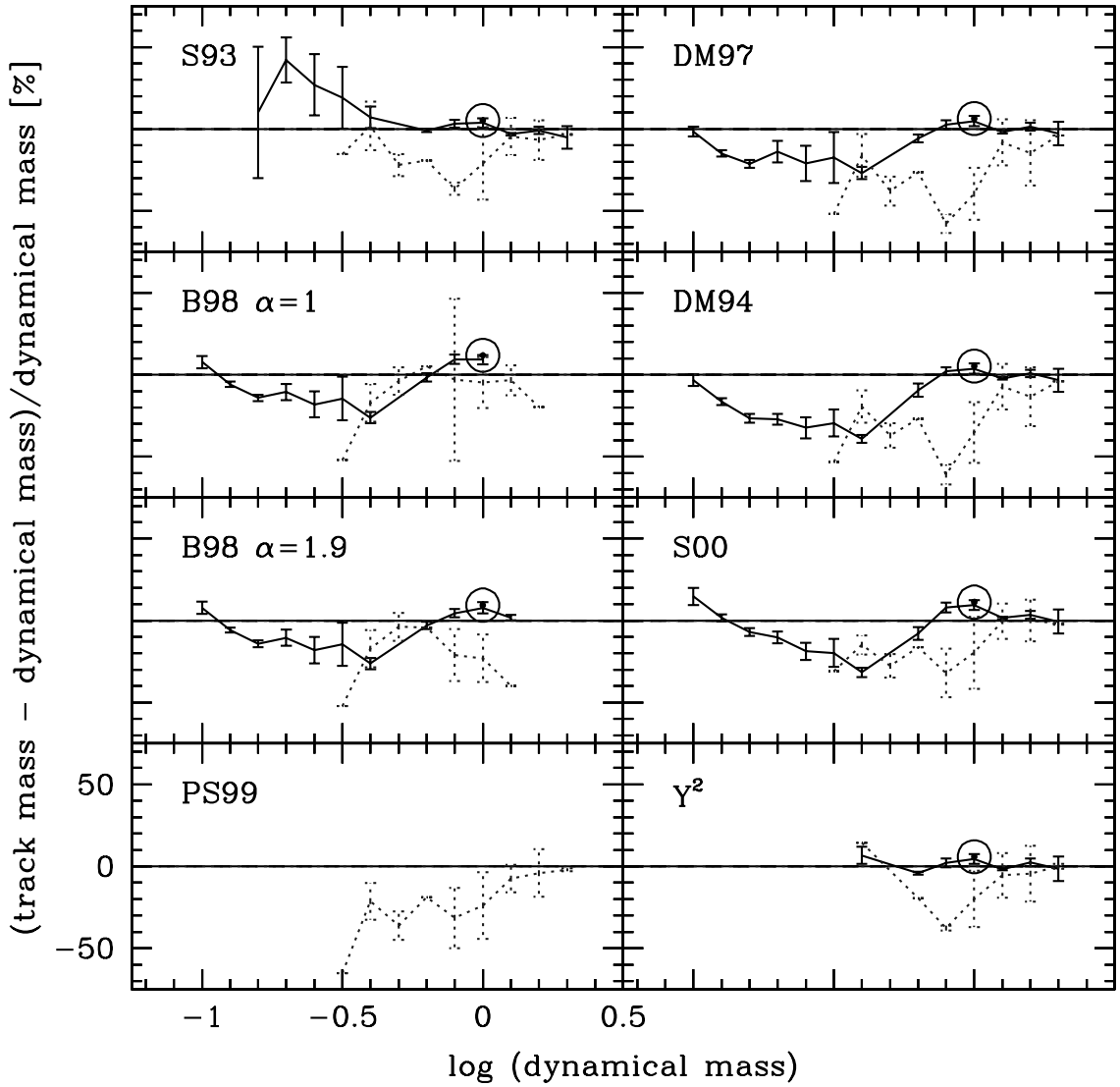

FIG. 5.—Mean percentage mass offset as a function of dynamically determined stellar mass for main-sequence (*solid lines*) and pre–main-sequence (*dotted lines*) stars; vertical error bars indicate the standard deviation of the mean. The difference values for the 4.5 Gyr old Sun are also shown as the large solar symbols. [*See the electronic edition of the Journal for a color version of this figure.*]

pre–main-sequence masses that are consistent with dynamically determined values to better than 1 σ in the mean (Fig. 5), with the DM94 and DM97 tracks tending to underpredict the individual masses by 0%–10%. Around 1 $M_{\odot}$ (0.5–1.2 $M_{\odot}$), the B98 $\alpha = 1.0$ models predict masses most consistent with dynamical values; the B98 $\alpha = 1.9$ and most other models predict masses that are too low by $\sim$25% at 1–2 σ, on average, compared to the dynamically determined values. This general trend of underpredicted masses continues (including for the B98 $\alpha = 1.0$ models) toward the lowest pre–main-sequence masses considered, 0.3 $M_{\odot}$, although with slightly less significance ($\sim$1 σ). Note that the valley of maximum disagreement between track-predicted and dynamical masses is driven for most models by two stars: UZ Tau Aa and NTTS 045251B.

Our assessment of these mass comparisons is limited by the accuracy with which our sample stars can be placed on an H-R diagram, particularly the youngest stars. As young solar- and lower mass stars are primarily on Hayashi (roughly constant temperature) evolutionary tracks, an accurate temperature is especially important for determining a theoretical mass. In our analysis we have adopted a dwarf temperature scale for both the main-sequence and the pre–main-sequence stars. Pre–main-sequence stars are intermediate-gravity objects between dwarfs and giants, and it has been argued (e.g., Martín, Rebolo, & Magazzù 1994; Luhman, Liebert, & Rieke 1997; White et al. 1999) that the appropriate spectral type–temperature relation of, in particular, T Tauri stars should be intermediate between that of dwarfs and giants. G and K giants are cooler than G and K dwarfs, while M giants are warmer than M dwarfs (see the Appendix for dwarf temperatures and Dyck et al. 1996, Di Benedetto & Rabbia 1987, and Bell & Gustafsson 1989 for giant temperatures derived from either angular diameters or the infrared flux method), with the crossover point at about M0. As examples, in comparison to dwarfs, giants of spectral type M6, M4, and M2 are $\sim$620, $\sim$500, and $\sim$310 K warmer, and K5 and K1 giants are $\sim$475 and $\sim$595 K cooler, respectively. Detailed analysis of high-dispersion spectra shows that pre–main-sequence surface gravities are closer to those of dwarfs than to those of giants. For example, Johns-Krull et al. (1999) measure $\log g = 3.67 \pm 0.5$ for BP Tau and Johns-Krull & Valenti (2000) quote $\log g = 3.54$ for Hubble 4. These values can be compared to $\log g = 4.6$ for a 4800 K dwarf and $\log g = 2.4$

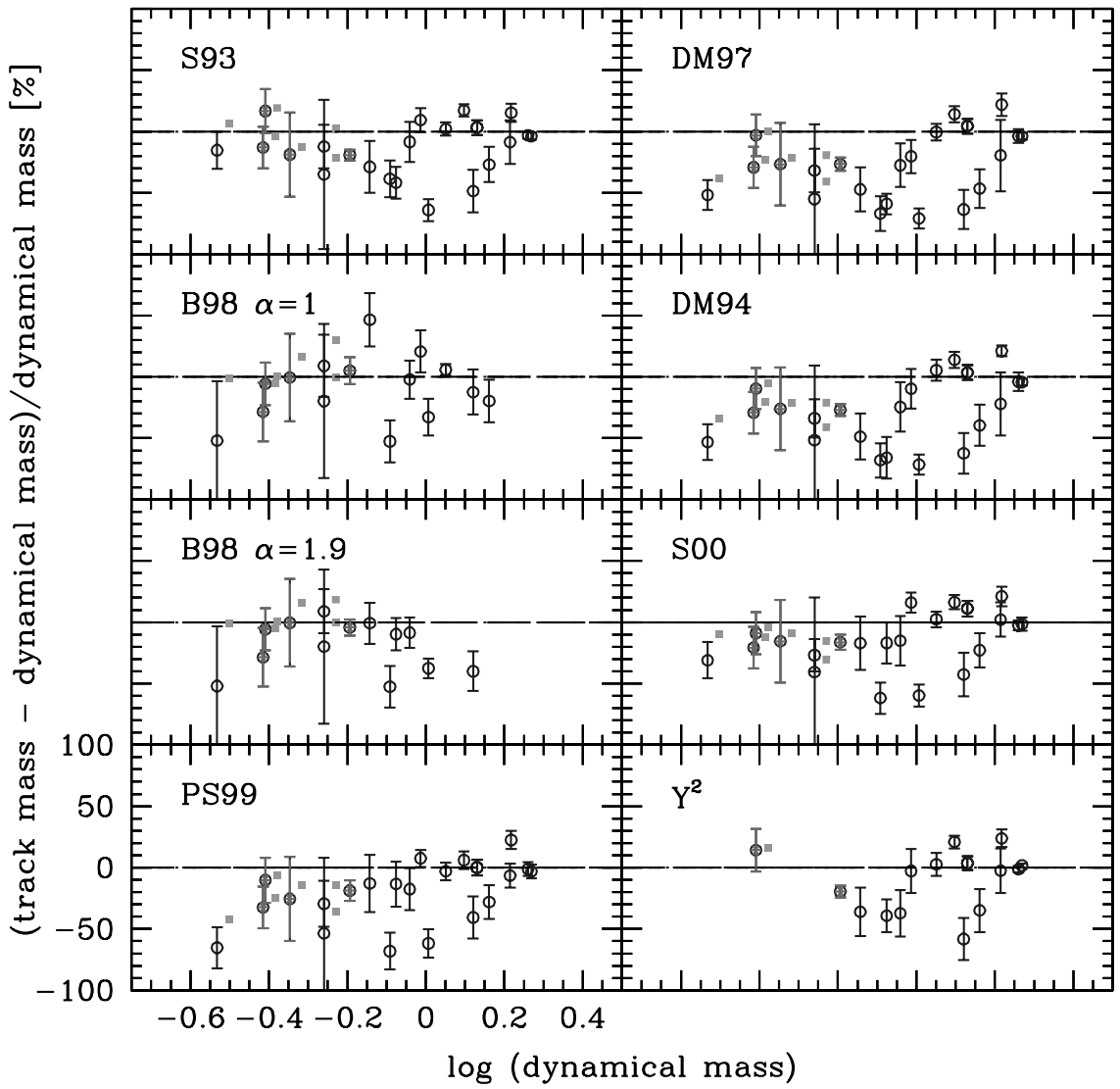

FIG. 6.—Percentage mass offset vs. dynamically determined stellar mass for individual pre–main-sequence stars. Vertical error bars indicate the root sum squared of the dynamical mass and the track mass error, the latter estimated from the $\log L$ and $\log T$ errors. To illustrate the effects of temperature scale choice, we show both the dwarf temperature scale adopted here (*circles*) and the warmer Luhman et al. (2003) temperature scale (*squares*) for stars later than M0, offset by +0.03 in log (dynamical mass) for clarity. Note the change in scale compared to Fig. 5. [*See the electronic edition of the Journal for a color version of this figure.*]

for a 4800 K giant (dwarf surface gravities staying roughly constant with decreasing temperature in the stellar range and giant gravities decreasing by 1 order of magnitude by 3900 K and 2 orders of magnitude by late M spectral types).

In our analysis, we have assumed a strict dwarflike temperature relation, since an appropriate temperature scale tied to the infrared flux method or measured stellar angular diameters has not yet been established for 1–10 Myr old low-mass stars. The systematic shift induced by adopting a temperature scale intermediate to those of dwarfs and giants would make our track-inferred masses for the pre–main-sequence stars *smaller* in the G–K spectral type range (the wrong direction for improving correspondence to dynamical masses) and *larger* by ~10% for the M types. Luhman et al. (2003) suggest a specific intermediate temperature scale for stars cooler than spectral type M0.[3] Using this warmer temperature scale for our pre–main-sequence sample (Fig. 6, *filled squares*) systematically increases the predicted masses of the lowest mass stars. However, there is no statistically significant evidence from dynamical mass constraints that a warmer-than-dwarf temperature scale is needed, since the resulting change in the predicted masses using a warmer scale is well within the uncertainties in the mass comparison plots (only two systems have masses shifted by $\geq 1\ \sigma$ via a change in the temperature scale).

Systematic shifts in the predicted masses, as would occur by shifting the temperature scale, will still leave many pre–main-sequence stars with track-predicted masses widely discrepant from dynamical values. This is illustrated by the large scatter in track-predicted masses over a small range of dynamically determined masses (Fig. 6). A couple of case studies make this point clear. Compare MWC 480, an A2 star with dynamical mass of $1.65 \pm 0.07\ M_{\odot}$, to the cooler but (surprisingly) more massive A8 stars RS Cha A and B, with dynamical masses of 1.858 ± 0.016 and $1.821 \pm 0.018\ M_{\odot}$, respectively. No evolutionary model will predict that a hotter object is less massive than a cooler object this close to the main sequence. Assuming that the uncertainties in the dynamical masses have

[3] The values of the Luhman intermediate temperature scale were chosen to produce coeval ages for the T Tauri quadruple GG Tauri and for members of the IC 348 cluster using the B98 ($\alpha = 1.9$) evolutionary models.

been properly assigned, this suggests that the assigned temperatures are in error. In this case, the error is most likely in the spectral type assigned to MWC 480, since RS Cha is an eclipsing system with more precisely determined temperatures. Similar discrepancies occur at lower masses. Consider NTTS 04251+3016A and LkCa 15, two K5 T Tauri stars with identical luminosities. Although these stars are located at the same position in the H-R diagram, they have dynamically determined masses that differ by 0.48 $M_\odot$, a 2.5 σ difference. This again strongly suggests errors in the assigned spectral types. These discrepancies are problems that will remain, independent of the temperature scale and independent of any evolutionary model. Assuming that the uncertainties in dynamical masses are being properly assessed, we conclude that the usefulness of dynamical mass constraints on pre–main-sequence evolutionary models is currently limited by poorly determined luminosities and especially temperatures of pre–main-sequence stars.

4.3. *Ensemble Comparisons*

Finally, in assessing the main-sequence and pre–main-sequence results en ensemble, we find it somewhat distressing that for most models the agreement is far better for main-sequence masses than for pre–main-sequence masses. Assuming that the stellar parameters on average are well understood (the above exceptions notwithstanding), apparently it is possible for stars of a given mass to wind up in the right place near the main-sequence end of a calculation without having started in the right place at the tops of their convective evolutionary tracks.

The B98 ($\alpha = 1.0$) models appear to have the best consistency between the pre–main-sequence and main-sequence mass offsets as a function of mass (Fig. 5), although we remind the reader that we found the B98 $\alpha = 1.0$ models a better fit to the pre–main sequence and the B98 $\alpha = 1.9$ models a better fit to the main sequence. If this trend is proved true, it may indicate a difference in the efficiency of convection between pre–main-sequence and main-sequence stars of similar mass. As noted above, for all models there is indeed *consistency* with dynamical masses above 1.2 $M_\odot$ in both the pre–main-sequence and the main-sequence phases; however, the pre–main-sequence masses are systematically offset by 0%–30% (<1 σ). Below 1 $M_\odot$ the consistency between the pre–main-sequence and main-sequence masses is broken, with the offset masses in the two regimes different in most models by more than 1 σ. Notably, it is in this subsolar regime that convection is most important, for an increasingly longer time period toward lower masses, during pre–main-sequence evolution.

5. CONCLUSIONS AND RECOMMENDATIONS

We have attempted to assess the agreement between dynamically determined stellar masses and those inferred from modern theoretical calculations of pre– and early–main-sequence evolution. We have found only marginal consistency with most existing models, as summarized in Figure 5.

For main-sequence stars, above 1.2 $M_\odot$ the models considered are all consistent with dynamically determined values. At lower masses, however, there is divergence between the predicted and dynamical masses, which sets in at different masses for different tracks. The Y^2 models offer the best overall agreement with dynamical masses, although these calculations extend only as low in mass as 0.4 $M_\odot$. The S93 models are a close second to the Y^2 models but begin to diverge from 1 σ consistency below 0.3 $M_\odot$. All other models (DM97, B98, S00, and PS99) fail to predict masses that are consistent with dynamically determined values (by 5%–20%) over the mass range 0.1–0.5 $M_\odot$. We find that for all tracks, the dominant discrepancies between track-predicted and dynamically determined masses for main-sequence stars lie in the mass range 0.2–0.5 $M_\odot$. This failure likely stems from the poor match to the empirically defined main sequence. The DM97, B98, PS99, and S00 models all predict a break in the mass-luminosity relationship near $\log T \sim 3.7$ dex (spectral type M0.5), which is hotter than the well-established empirical break in the mass-luminosity relationship near $\log T \sim 3.5$ dex (spectral type M3.5). The S93 and Y^2 models most closely resemble the empirical main sequence.

For the pre–main-sequence sample, we find generally good agreement between predicted and dynamical masses above 1.2 $M_\odot$ for all models, as was true for the main-sequence sample. This is not an entirely trivial statement, since both partially convective and fully radiative stars are included in these two samples. However, referring to Figure 1, differences between the various models for 1–2 $M_\odot$ stars are manifest only high on the fully convective part of the tracks, where no empirical data exist; thus, even younger 1–2 $M_\odot$ dynamical masses are needed before distinction between the pre–main-sequence tracks can be made in this mass regime. Between 1.2 and 0.5 $M_\odot$, the B98 ($\alpha = 1.0$) models predict *reasonable*, although not fully consistent, mass values on average, while all other models systematically underestimate subsolar masses by 10%–30%, on average. At the lowest masses considered, $\lesssim$0.5 $M_\odot$, all models underestimate the pre–main-sequence stellar masses. There are at present no dynamical mass constraints available at masses less than 0.3 $M_\odot$ for pre–main-sequence stars. Adopting a warmer-than-dwarf temperature scale for T Tauri stars could partly reconcile these mass underestimates, although the scale proposed by Luhman et al. (2003) is not warm enough to rectify the mass underestimates except for the marginal (i.e., not statistically significant) improvements made to the B98 model agreement (the models to which this temperature scale was in fact tuned). Of note is that the B98 models do not extend above radii of 1–2 $R_\odot$ (specifically, the 10^6 yr isochrone), whereas many young pre–main-sequence stars have larger radii, 2–3 $R_\odot$, thus limiting the utility of the B98 models in star-forming regions. The dynamical mass consistency of the B98 models is only marginally better than that of the DM97, PS99, and S00 models, which systematically underestimate subsolar masses by 1–2 σ.

The relatively flat nature of the offsets between the dynamical and the predicted stellar masses for some calculations suggests that they could be used with moderate confidence if correction factors are included. For example, a 20% revision upward of the masses predicted by the DM97 tracks for masses between 0.12–0.4 $M_\odot$ would result in near-perfect agreement at main-sequence evolutionary stages, with the same 20% correction applicable to 0.3–1.0 $M_\odot$ young pre–main-sequence stars; again we note that the pre–main-sequence behavior below 0.3 $M_\odot$ is untested for these or any set of tracks. A similar 20% correction could be applied to the S00 pre–main-sequence tracks, although the main-sequence offsets appear to vary with mass.

Several observational recommendations can also be made. Our pre–main-sequence comparisons stress the need for more observational work on masses determined from orbital dynamics in the pre–main-sequence phase, where the statistics of our assembled sample are factors of 5–10 worse than on the main sequence at comparable masses. This is especially problematic at

the lowest masses, where at present there are no pre–main-sequence dynamical mass constraints at masses of less than 0.3 $M_\odot$. Finally, we emphasize that the usefulness of dynamical mass constraints on pre–main-sequence evolutionary models is currently limited by poorly determined luminosities and especially temperatures of young stars. Additional dynamical mass determinations will not likely improve the constraints on evolutionary models, unless the stellar parameters can be more accurately determined than for the current sample. In the absence of additional eclipsing systems, high-dispersion stellar spectroscopy and synthetically modeled spectra offer the best promise for precisely determining fundamental properties.

The trends that have emerged from our study may be interpretable as messages regarding modifications to the model assumptions on input physics and parameter choices. It is suggested that in order to achieve agreement between dynamical and track-predicted masses for both low-mass young pre–main-sequence and main-sequence stars, a systematic shift coolward of the models via improved convection and opacity treatments is needed. Further adjustments may also be necessary. Baraffe and coworkers have repeatedly stressed the important effects of atmospheres at low masses, arguing that the gray (Eddington) approximation used by most other authors overestimates both the temperature and the luminosity for a given mass. This could explain in part some of the discrepancies between the predicted and empirical main sequences (Fig. 2). It is worth noting that the deviations occur near early M spectral types, where molecular absorption begins to dominate the opacity. However, even the nongray atmospheres of the B98 models fail to reproduce the empirical main sequence. For the pre–main-sequence stars, although the physics involved in opacities, equations of state, and atmospheric treatment is already challenging, even more sophisticated effects, such as accretion, rotation, and magnetic fields, may be required in order to achieve rigorous agreement between observations and models, as illustrated by e.g., D'Antona et al. (2000) and Baraffe et al. (2002).

Note added in manuscript.—Stassun et al. (2004) report dynamical mass measurements for a pre–main-sequence system consisting of 1.01 and 0.73 $M_\odot$ components. We have included this system in our table for completeness, but it does not appear in our figures or analysis. Results from this new dynamical mass system are consistent with those for other pre–main-sequence stars with similar masses.

We acknowledge useful comments by the referee.

APPENDIX

ADOPTED DWARF TEMPERATURES AND BOLOMETRIC CORRECTIONS

As discussed in the text (§§ 3.3 and 4.2), we have adopted a dwarf temperature scale based on the stellar temperatures of Chlebowski & Garmany (1991) (O3–O9); Humphreys & McElroy (1984) (B0–B3); Cohen & Kuhi (1979) (B5–K6); Bessell (1991) (K7–M1); Wilking, Greene, & Meyer (1999) (M2–M7.5); and Reid et al. (1999) and Burgasser (2001) (M8–L–T). Our bolometric corrections are those of Massey, Parker, & Garmany (1989) (O3–B1); Code et al. (1976) (B2–G0); Bessell (1991) and Bessell & Brett (1988) (G0–M5); and Tinney, Mould, & Reid (1993) (M6–M9, converted from quoted values of *K*-band bolometric correction). The *V*-band bolometric corrections turn over at spectral types later than late G and grow rapidly as flux shifts from the *V* band into redder bandpasses. The *I* band is generally the best wavelength at which to apply a bolometric correction for stars in the early K through mid-M spectral type range, both because the value of the bolometric correction is small and because it is roughly constant with spectral type. For very late M-types, the *J* band may be a better choice.

REFERENCES

Alencar, S. H. P., Melo, C. H. F., Dullemond, C. P., Andersen, J., Batalha, C., Vaz, L. P. R., & Mathieu, R. D. 2003, A&A, 409, 1037
Alexander, D. R., Augason, G. C., & Johnson, H. R. 1989, ApJ, 345, 1014
Alexander, D. R., & Ferguson, J. W. 1994, ApJ, 437, 879
Andersen, J. 1991, A&A Rev., 3, 91
Andersen, J., Lindgren, H., Hazen, M. L., & Mayor, M. 1989, A&A, 219, 142
Bahcall, J. N., & Pinsonneault, M. H. 1992, Rev. Mod. Phys., 64, 885
Baraffe, I., Chabrier, G., Allard, F., & Hauschildt, P. H. 1995, ApJ, 446, L35
———. 1998, A&A, 337, 403 (B98)
———. 2002, A&A, 382, 563
Basri, G., & Batalha, C. 1990, ApJ, 363, 654
Bell, R. A., & Gustafsson, B. 1989, MNRAS, 236, 653
Bernasconi, P. A. 1996, A&AS, 120, 57
Bessell, M. S. 1991, AJ, 101, 662
Bessell, M. S., & Brett, J. M. 1988, PASP, 100, 1134
Böhm-Vitense, E. 1958, Z. Astrophys., 46, 108
Burgasser, A. J. 2001, Ph.D. thesis, Caltech
Burrows, A., et al. 1997, ApJ, 491, 856
Canuto, V. M., & Mazzitelli, I. 1991, ApJ, 370, 295
———. 1992, ApJ, 389, 724
Casey, B. W., Mathieu, R. D., Vaz, L. P. R., Andersen, J., & Suntzeff, N. B. 1998, AJ, 115, 1617
Caughlan, G. R., & Fowler, W. A. 1988, At. Data Nucl. Data Tables, 40, 283
Chabrier, G., & Baraffe, I. 1997, A&A, 327, 1039
Chabrier, G., Baraffe, I., Allard, F., & Hauschildt, P. 2000, ApJ, 542, 464
Charbonnel, C., Däppen, W., Schaerer, D., Bernasconi, P. A., Maeder, A., Meynet, G., & Mowlavi, N. 1999, A&AS, 135, 405
Chlebowski, T., & Garmany, C. D. 1991, ApJ, 368, 241
Code, A. D., Davis, J., Bless, R. C., & Brown, R. H. 1976, ApJ, 203, 417
Cohen, M., & Kuhi, L. V. 1979, ApJS, 41, 743
Copeland, H., Jensen, J. O., & Jørgensen, H. E. 1970, A&A, 5, 12
Covino, E., et al. 2000, A&A, 361, L49
Cox, A. N., ed. Allen's Astrophysical Quantities 2000 (4th ed.; New York: Springer)
Cox, A. N., & Tabor, J. E. 1976, ApJS, 31, 271
Cox, J. P., & Giuli, R. T. 1968, Principles of Stellar Structure (New York: Gordon & Breach)
D'Antona, F., & Mazzitelli, I. 1985, ApJ, 296, 502
———. 1994, ApJS, 90, 467 (DM94)
———. 1997, Mem. Soc. Astron. Italiana, 68, 807 (DM97)
D'Antona, F., Ventura, P., & Mazzitelli, I. 2000, ApJ, 543, L77
Däppen, W., Mihalas, D., Hummer, D. G., & Mihalas, B. W. 1988, ApJ, 332, 261
Delfosse, X., Forveille, T., Ségransan, D., Beuzit, J.-L., Udry, S., Perrier, C., & Mayor, M. 2000, A&A, 364, 217
Di Benedetto, G. P., & Rabbia, Y. 1987, A&A, 188, 114
Dutrey, A., Guilloteau, S., & Simon, M. 2003, A&A, 402, 1003
Dyck, H. M., Benson, J. A., van Belle, G. T., & Ridgway, S. T. 1996, AJ, 111, 1705
Eggleton, P. P., Faulkner, J., & Flannery, B. P. 1973, A&A, 23, 325
Ezer, D., & Cameron, A. G. W. 1967a, Canadian J. Phys., 45, 3429
———. 1967b, Canadian J. Phys., 45, 3461
Fernandes, J., Lebreton, Y., Baglin, A., & Morel, P. 1998, A&A, 338, 455
Forestini, M. 1994, A&A, 285, 473
Fowler, W. A., Caughlan, G. R., & Zimmerman, B. A. 1975, ARA&A, 13, 69
Giménez, A., & Quintana, J. M. 1992, A&A, 260, 227

Girardi, L., Bressan, A., Bertelli, G., & Chiosi, C. 2000, A&AS, 141, 371
Gray, D. F. 1992, The Observation and Analysis of Stellar Photospheres (2nd ed.; Cambridge: Cambridge Univ. Press)
———. 1994, PASP, 106, 1248
Griffin, R. F. 1985, Observatory, 105, 226
Gruzinov, A. V., & Bahcall, J. N. 1998, ApJ, 504, 996
Guenther, D. B., & Demarque, P. 2000, ApJ, 531, 503
Guenther, D. B., Demarque, P., Kim, Y.-C., & Pinsonneault, M. H. 1992, ApJ, 387, 372
Harris, M. J., Fowler, W. A., Caughlan, G. R., & Zimmerman, B. A. 1983, ARA&A, 21, 165
Hartigan, P., Edwards, S., & Ghandour, L. 1995, ApJ, 452, 736
Hartigan, P., & Kenyon, S. J. 2003, ApJ, 583, 334
Hartigan, P., Strom, K., & Strom, S. 1994, ApJ, 427, 961
Hartmann, L., Cassen, P., & Kenyon, S. J. 1997, ApJ, 475, 770
Hauschildt, P. H., Allard, F., & Baron, E. 1999, ApJ, 512, 377
Heiter, U., et al. 2002, A&A, 392, 619
Herbig, G. H., Vrba, F. J., & Rydgren, A. E. 1986, AJ, 91, 575
Hummer, D. G., & Mihalas, D. 1988, ApJ, 331, 794
Humphreys, R. M., & McElroy, D. B. 1984, ApJ, 284, 565
Iben, I., Jr. 1965, ApJ, 141, 993
Iglesias, C. A., & Rogers, F. J. 1996, ApJ, 464, 943
Jaschek, M., Jaschek, C., & Andrillat, Y. 1988, A&AS, 72, 505
Johns-Krull, C. M., & Valenti, J. A. 2000, in ASP Conf. Ser. 198, Stellar Clusters and Associations: Convection, Rotation, and Dynamos, ed. R. Pallavicini, G. Micela, & S. Sciortino (San Francisco: ASP), 371
Johns-Krull, C. M., Valenti, J. A., & Koresko, C. 1999, ApJ, 516, 900
Kenyon, S. J., Dobrzycka, D., & Hartmann, L. 1994, AJ, 108, 1872
Kim, Y.-C., Demarque, P., Yi, S. K., & Alexander, D. R. 2002, ApJS, 143, 499
Kurucz, R. L. 1991, in Stellar Atmospheres: Beyond Classical Models, ed. L. Crivellari, I. Hubeny, & D. G. Hummer (Dordrecht: Kluwer), 441
Lacy, C. H. S. 1997a, AJ, 113, 1406
———. 1997b, AJ, 113, 1091
———. 1997c, AJ, 114, 2140
Lacy, C. H. S., Torres, G., Latham, D. W., Zakirov, M. M., & Arzumanyants, G. C. 1997, AJ, 114, 1206
Larson, R. B. 1972, MNRAS, 156, 437
Lastennet, E., & Valls-Gabaud, D. 2002, A&A, 396, 551
Latham, D. W., Nordström, B., Andersen, J., Torres, G., Stefanik, R. P., Thaller, M., & Bester, M. J. 1996, A&A, 314, 864
Lejeune, T., Cuisinier, F., & Buser, R. 1998, A&AS, 130, 65
Liu, Q., & Yang, Y. 2000, A&A, 361, 226
Luhman, K. L., Liebert, J., & Rieke, G. H. 1997, ApJ, 489, L165
Luhman, K. L., Stauffer, J. R., Muench, A. A., Rieke, G. H., Lada, E. A., Bouvier, J., & Lada, C. J. 2003, ApJ, 593, 1093
Magni, G., & Mazzitelli, I. 1979, A&A, 72, 134
Mamajek, E. E., Lawson, W. A., & Feigelson, E. D. 1996, AJ, 112, 276
Marrese, P. M., Munari, U., Siviero, A., Milone, E. F., Zwitter, T., Tomov, T., Boschi, F., & Boeche, C. 2004, A&A, 413, 635
Martín, E. L., Rebolo, R., & Magazzù, A. 1994, ApJ, 436, 262
Mason, B. D., McAlister, H. A., & Hartkopf, W. I. 1996, AJ, 112, 276
Massey, P., Parker, J. W., & Garmany, C. D. 1989, AJ, 98, 1305
McAlister, H. A., Hartkopf, W. I., Mason, B. D., Fekel, F. C., Ianna, P. A., Tokovinin, A. A., Griffin, R. F., & Culver, R. B. 1995, AJ, 110, 366
Mendes, L. T. S., D'Antona, F., & Mazzitelli, I. 1999, A&A, 341, 174
Mercer-Smith, J. A., Cameron, A. G. W., & Epstein, R. I. 1984, ApJ, 279, 363
Metcalfe, T. S., Mathieu, R. D., Latham, D. W., & Torres, G. 1996, ApJ, 456, 356
Mihalas, D., Däppen, W., & Hummer, D. G. 1988, ApJ, 331, 815
Milone, E. F., Stagg, C. R., & Kurucz, R. L. 1992, ApJS, 79, 123
Montalbán, J., D'Antona, F., Kupka, F., & Heiter, U. 2004, A&A, in press
Munari, U., et al. 2001, A&A, 378, 477
North, P., Studer, M., & Künzli, M. 1997, A&A, 324, 137
Palla, F., & Stahler, S. W. 1993, ApJ, 418, 414
———. 1999, ApJ, 525, 772 (PS99)
Plez, B. 1992, A&AS, 94, 527
Pols, O. R., Tout, C. A., Eggleton, P. P., & Han, Z. 1995, MNRAS, 274, 964
Popper, D. M. 1987, ApJ, 313, L81
———. 1994, AJ, 108, 1091
———. 1997, AJ, 114, 1195
Pourbaix, D. 2000, A&AS, 145, 215
Prato, L., Greene, T. P., & Simon, M. 2003, ApJ, 584, 853
Prato, L., Simon, M., Mazeh, T., Zucker, S., & McLean, I. S. 2002, ApJ, 579, L99
Reid, I. N., et al. 1999, ApJ, 521, 613
Ribas, I. 2003, A&A, 398, 239
Ribas, I., Jordi, C., & Torra, J. 1999, MNRAS, 309, 199
Ribas, I., Jordi, C., Torra, J., & Giménez, Á. 2000, MNRAS, 313, 99
Rogers, F. J., & Iglesias, C. A. 1992, ApJS, 79, 507
Rogers, F. J., Swenson, F. J., & Iglesias, C. A. 1996, ApJ, 456, 902
Saumon, D., Chabrier, G., & Van Horn, H. M. 1995, ApJS, 99, 713
Schaefer, G. H., Simon, M., Nelan, E., & Holfeltz, S. T. 2003, AJ, 126, 1971
Ségransan, D., Delfosse. X., Forveille, T., Beuzit, J.-L., Udry, S., Perrier, C., & Mayor, M. 2000, A&A, 364, 665
Siess, L., Dufour, E., & Forestini, M. 2000, A&A, 358, 593 (S00)
Siess, L., Forestini, M., & Bertout, C. 1997, A&A, 326, 1001
Siess, L., & Livio, M. 1997, ApJ, 490, 785
Sills, A., Pinsonneault, M. H., & Terndrup, D. M. 2000, ApJ, 534, 335
Simon, M., Dutrey, A., & Guilloteau, S. 2000, ApJ, 545, 1034
Stahler, S. W. 1983, ApJ, 274, 822
Stassun, K. G., Mathieu, R. D., Vaz, L. P. R., Stroud, N., & Vrba, F. J. 2004, ApJS, 151, 357
Stauffer, J. R., Hartmann, L. W., & Barrado y Navascués, D. 1995, ApJ, 454, 910
Steffen, A. T., et al. 2001, AJ, 122, 997
Strassmeier, K. G., Hall, D. S., Fekel, F. C., & Scheck, M. 1993, A&AS, 100, 173
Stüwe, J. A., & Schulz, R. 1994, Astron. Nachr., 315, 427
Swenson, F. J., Faulkner, J., Rogers, F. J., & Iglesias, C. A. 1994, ApJ, 425, 286 (S93)
Tamazian, V. S., Docobo, J. A., White, R. J., & Woitas, J. 2002, ApJ, 578, 925
Tinney, C. G., Mould, J. R., & Reid, I. N. 1993, AJ, 105, 1045
Tomkin, J., McAlister, H. A., Hartkopf, W. I., & Fekel, F. C. 1987, AJ, 93, 1236
Torres, G., Boden, A. F., Latham, D. W., Pan, M., & Stefanik, R. P. 2002, AJ, 124, 1716
Torres, G., Henry, T. J., Franz, O. G., & Wasserman, L. H. 1999, AJ, 117, 562
Torres, G., & Ribas, I. 2002, ApJ, 567, 1140
Torres, G., Stefanik, R. P., Andersen, J., Nordström, B., Latham, D. W., & Clausen, J. V. 1997a, AJ, 114, 2764
Torres, G., Stefanik, R. P., & Latham, D. W. 1997b, ApJ, 485, 167
Valenti, J. A., Basri, G., & Johns, C. M. 1993, AJ, 106, 2024
VandenBerg, D. A. 1983, ApJS, 51, 29
———. 1992, ApJ, 391, 685
VandenBerg, D. A., & Clem, J. L. 2003, AJ, 126, 778
VandenBerg, D. A., Swenson, F. J., Rogers, F. J., Iglesias, C. A., & Alexander, D. R. 2000, ApJ, 532, 430
Viti, S., Jones, H. R. A., Schweitzer, A., Allard, F., Hauschildt, P. H., Tennyson, J., Miller, S., & Longmore, A. J. 1997, MNRAS, 291, 780
White, R. J., Ghez, A. M., Reid, I. N., & Schultz, G. 1999, ApJ, 520, 811
Wilking, B. A., Greene, T. P., & Meyer, M. R. 1999, AJ, 117, 469
Yi, S., Demarque, P., Kim, Y.-C., Lee, Y.-W., Ree, C. H., Lejeune, T., & Barnes, S. 2001, ApJS, 136, 417
Yi, S. K., Kim, Y.-C., & Demarque, P. 2003, ApJS, 144, 259
Zwitter, T., Munari, U., Marrese, P. M., Prsa, A., Milone, E. F., Boschi, F., Tomov, T., & Siviero, A. 2003, A&A, 404, 333